Cistromic reprogramming of the diurnal glucocorticoid hormone response by high fat diet

Fabiana Quagliarini [1], Ashfaq Ali Mir [1], Kinga Balazs [1,3], Michael Wierer [2], Kenneth Allen Dyar [1], Celine Jouffe [1], Konstantinos Makris [1], Johann Hawe [4], Matthias Heinig [4], Fabian Volker Filipp [4], Grant Daniel Barish [5] and Nina Henriette Uhlenhaut [1,6,7]

1: Institutes for Diabetes & Obesity and Diabetes & Cancer, IDO/IDC, Helmholtz Center Munich (HMGU) and German Center for Diabetes Research (DZD), Ingolstaedter Landstr. 1, 85764 Neuherberg (Munich), Germany

2: Department of Proteomics and Signal Transduction, Max Planck Institute of Biochemistry, 82152 Martinsried, Germany

3: Institute of Bioinformatics and Systems Biology (IBIS) & 4: Institute of Computational Biology (ICB), HMGU, Ingolstaedter Landstr. 1, 85764 Neuherberg, Munich, Germany

5: Department of Medicine, Division of Endocrinology, Metabolism and Molecular Medicine, Northwestern University Feinberg School of Medicine, Chicago, IL 60611, USA

6: Metabolic Biochemistry and Genetics, Gene Center, Ludwig Maximilians Universitaet (LMU), Feodor Lynen Str. 25, 81377 Munich, Germany

[7] corresponding author / lead contact:

N. Henriette Uhlenhaut, henriette.uhlenhaut@helmholtz-muenchen.de

Summary

The Glucocorticoid Receptor (GR) is a potent metabolic regulator and a major drug target. While GR is known to play integral roles in circadian biology, its rhythmic genomic actions have never been characterized. Here we mapped GR's chromatin occupancy in mouse livers throughout the day/night cycle. We show how GR partitions metabolic processes by time-dependent target gene regulation, and how GR controls circulating glucose and triglycerides differentially during feeding and fasting. Highlighting the dominant role GR plays in synchronizing circadian amplitudes, we find that the majority of oscillating genes are bound by and depend on GR. This rhythmic pattern is altered by high fat diet in a ligand-independent manner. We find that the remodeling of oscillatory gene expression and of postprandial GR binding result from a concomitant increase of STAT5 co-occupancy in obese mice. Altogether, our findings highlight GR's fundamental role in the rhythmic orchestration of hepatic metabolism.

Keywords

Glucocorticoid Receptor, mouse liver, circadian clock, cistromes, PPARα, Stat5, glucose and lipid metabolism, high fat diet

Introduction

Circadian rhythms drive the physiological adaptation to daily phases of resting/fasting and activity/feeding (Eckel-Mahan and Sassone-Corsi, 2013; Panda, 2016). At molecular level, the circadian clock consists of a 24-hour feedback loop, in which the activators CLOCK and BMAL1 (ARNTL) induce their own repressors, CRY1/2 and PER1/2/3. A second loop is formed by the nuclear receptors REV-ERBα/β (NR1D1/2) and RORα/β/γ (RORA/B/C) (Takahashi, 2017).

Glucocorticoids (GCs) are steroid hormones secreted with a prominent circadian rhythm. GCs peak at the onset of the feeding phase, occurring in the early night in rodents, and in the early morning in humans (Spiga et al., 2014). GCs maintain blood glucose during periods of stress or fasting and entrain metabolic programs among different organs (Patel et al., 2014). It has been shown that GCs can synchronize daily rhythmicity in peripheral tissues and that treating cells and mice with GCs induces circadian gene expression and corresponding oscillations (Balsalobre et al., 2000; Oishi et al., 2005; Reddy et al., 2007).

GCs bind to the Glucocorticoid Receptor (GR; NR3C1), a ligand gated transcription factor belonging to the nuclear receptor superfamily. Upon hormone binding, GR enters the nucleus to regulate gene expression by direct binding to glucocorticoid response elements (GREs) in the DNA of target promoters or enhancers (Greulich et al., 2016). Several studies have shown both genetic and physical interactions between GR and the core clock machinery: For example, functional GREs have been identified in the *Per1* and *Per2* regulatory regions, while the *Rev-erbα* promoter was found to be repressed by GR (So et al., 2009; Torra et al., 2000; Yamamoto et al., 2005). CRY1 and CRY2 were shown to interact with GR in a ligand-dependent manner to repress the activation of gluconeogenic genes like *Pck1* (Lamia et al., 2011). Similarly, CLOCK antagonizes GC-induced transcriptional activity via lysine acetylation of the GR protein itself (Nader et al., 2009).

Disruption of either clock function or GC secretion causes profound metabolic dysregulation, resulting in obesity, type 2 diabetes, and nonalcoholic fatty liver disease (Eckel-Mahan and Sassone-Corsi, 2013; Marcheva et al., 2013). On the other hand, GC excess has detrimental effects on glucose and fat metabolism (Patel et al., 2014). Finally, there is a bifacial relationship between metabolism and the clock, as the internal time keepers are very sensitive to changes in the nutritional environment. For instance, it has been shown that excessive caloric intake (just like time restricted feeding) can shift circadian patterns of transcription and energetics (Damiola et al., 2000; Eckel-Mahan et al., 2013). (Bass, 2016). Thus, circadian misalignment from inappropriate feeding schedules or shift work is associated with metabolic disease and altered GC rhythmicity (Barclay et al., 2012; Spiegel et al., 2009).

Despite much evidence for a role for GR in circadian biology, its actual contribution to diurnal rhythms has not been studied on a genomic scale. We used ChIP-Seq, RNA-Seq, proteomics and mouse genetics to characterize hepatic GR function around the clock. Here we show that the daily rhythm of corticosterone secretion has a differential effect on chromatin occupancy by GR. We find that GR regulates nutrient partitioning by binding to promoter proximal sites near housekeeping and gluconeogenic genes during the day, while the nightly GC surge allows GR to reach distant enhancers activating lipid and amino acid metabolism. The majority of 24 hour oscillating genes are bound by GR in a time point specific manner overlapping with core clock factors. Surprisingly, this rhythmic pattern is altered by nutritional challenge. Exposure to high fat diet (HFD) causes an expansion of the GR cistrome selectively during the night. This concurs with remodeling of target gene expression and an increased crosstalk with Stat5 signaling. By using liver specific knockout mice, we demonstrate that these GR-dependent temporal metabolic gene programs affect circulating glucose and triglycerides respectively during feeding and fasting. Furthermore, we observe an altered response to exogenous GCs in obese mice. Taken together, we provide evidence that nutrition influences the clock and the GC response in a ligand-independent fashion.

Results

GR binding to chromatin is rhythmic

To investigate the genomic extent of circadian gene regulation by GR, we performed ChIP-Seq on mouse livers every 4 hours throughout the day and night cycle. Our experimental cohort showed the expected rise in corticosterone levels towards ZT12 (lights off), with lowest levels being detected at ZT0 (lights on) (Figure S1A). We detected binding of GR to its known hepatic target genes, such as *Per1* in all replicates (Figure 1A and data not shown). For our analyses, normalized ChIP-Seq data from two biological replicates were used for peak calling. We then created a 'peak union' of 14,920 genomic sites reproducibly bound by GR at any given time point. Subsequently, we quantified occupancy from the sequencing tag counts for all peaks within the union for each time point.

Interestingly, it appears that the strength of the ChIP-Seq signal mirrored the endogenous ligand availability, with peak GR occupancy coinciding with the highest levels of hormone secretion (Figures 1A&B and S1A&B). The highest number of GR-bound loci was found at ZT12, at the beginning of the active/feeding phase and at the peak of corticosterone secretion. Afterwards, at ZT16 and 20, these numbers dropped, to reach the lowest amount of GR-bound *cis*-regulatory elements during the day (ZT0, 4 and 8). GR binding largely occurred near gene bodies during this phase, meaning that high-affinity sites bound during the day under low hormone levels, were primarily at the promoter. During the night (ZT12, 16 and 20), increased ligand availability seemed to enable GR to reach distant enhancers, and a larger fraction of ChIP peaks could be detected at greater distance from the transcription start site (Figure 1C and S1C). Approximately 800 GR binding sites consistently mapped to <1kb upstream of the TSS during both day and night, while the number of distal intergenic elements increased from <500 during the day to >2,000 at night.

To further characterize these target sites, we grouped the first three (lights on, ZT 0, 4, 8) and the last three (lights off, ZT 12, 16, 20) time points together. Figure 1D shows that most of the GR binding

sites occupied during fasting were also bound during the feeding phase. Functionally, these promoter proximal sites corresponded to house-keeping genes involved in chromatin organization, gene expression and cellular maintenance. Consistent with its known role in gluconeogenesis, 'glucose metabolism' was an enriched term. The majority of GR sites (roughly 10,000), however, which were occupied *only* at night and which include distal elements, were linked to genes important for amino acid and cholesterol metabolism, fatty acid and triglyceride metabolism. Hence, metabolic gene expression programs were regulated by GR in response to hormone specifically at night, while the mice were moving, eating and digesting their food (Figures 1D, and S1D-F).

Motif analyses revealed a significant enrichment for known co-occurring liver specific transcription factors, such as HNF4α, C/EBP, FoxA and HNF6 (Lim et al., 2015) at all times. We also newly identified PPAR (and CREB) response elements near GREs in our cistromes. Promoter proximal 'high affinity' sequences occupied during both day and night were further enriched for ETS transcription factor motifs and showed a higher percentage of 'perfect' GREs, whereas the distal sites bound only at night additionally featured HNF1 motifs and fewer consensus GREs (Figures 1E-G, and S1G).

In summary, our ChIP-Seq experiments around the clock in mouse livers showed that GR chromatin occupancy followed a daily rhythm aligned with its ligand availability. Low hormone levels during the day resulted in promoter proximal binding near housekeeping and gluconeogenic genes, while high corticosterone during the night brought about additional binding to distal regulatory elements near lipid metabolic target genes.

GR binding overlaps with core clock factors and drives rhythmic transcription

Since GR activity is tightly connected with circadian rhythms, we integrated our data sets with published liver cistromes for the core clock machinery (Koike et al., 2012). We calculated the peak overlap for our GR ChIP-sequences with CLOCK, BMAL1, PER1, PER2, CRY1 and CRY2 ChIP-signals from each time point. We then performed functional annotation of co-bound promoters and

enhancers by association with the nearest coding gene. As shown in Figure 2A, GR binding only partially overlapped with CLOCK and BMAL1, given that they primarily act during the day, while GR mainly appears at night. In order to characterize commonly regulated genes, irrespective of the phase of genomic binding, we performed functional annotation of all co-bound promoters and enhancers by association with the nearest protein coding gene. The genes co-occupied in sum by GR together with CLOCK/BMAL1 were involved in carbohydrate, lipid and amino acid metabolism, as well as circadian clock function, consistent with their roles in metabolic regulation (Figure 2B).

Both GCs and BMAL1/CLOCK are potent inducers of *Per1* and *Per2* expression. Consequently, we found co-occupancy of *cis*-regulatory elements by GR, PER1 and PER2 mostly at ZT12, 16 and 20, with GR slightly preceding *Per1/Per2* (Figure 2C). The genes commonly regulated during the night were assigned to lipid and amino acid metabolism, circadian clock function and Notch signaling (Figure 2D). Again, this underscores the link between GCs, the clock and metabolic homeostasis.

GR has previously been reported to physically interact with CRY1/2 in mouse livers (Lamia et al., 2011). Accordingly, we observed the largest overlap among all the clock factors for GR, CRY1 and CRY2. Similar to PER1 and PER2, GR binding coincided with cryptochromes predominantly at ZT12 and during the remainder of the dark phase (Figure 2E). Again, the gene networks that could be linked to these co-bound enhancers regulated lipid and amino acid metabolism, clock function as well as Srebp targets (Figure 2F).

In addition, we used ChIP-Seq data sets for REV-ERB-α/β and RORα/γ (Cho et al., 2012; Fang et al., 2014; Zhang et al., 2015) to determine the potential impact of GR on this regulatory loop (Figure S2A). Both REV-ERBs peak at ZT8, before being repressed by GR, while RORs peak at night (Bookout et al., 2006; Yang et al., 2006). Both REV-ERBα/β and RORα/γ significantly overlapped with GR at common enhancers and promoters. GR and REV-ERBα/β co-bound approximately 6,000 sites, of which about 5,000 sites were identically co-occupied by GR and RORα/γ. Of course these events did not happen simultaneously, but rather sequentially. These core *cis*-regulatory sequences targeted by

GR and the Rev-erb-ROR loop again corresponded to genes involved in lipid, fatty acid and amino acid metabolism, the circadian clock and PPARα activity.

Taken together, we found that GR occupancy partially overlapped with the classical clock transcription factors, most prominently with cryptochromes and with the ancillary loop, in a rhythmic pattern, at loci governing glucose, lipid and amino acid metabolism. One predominant theme among all the GR and 'clock' co-occupied target genes was an enrichment for PPAR signaling (Figures 2B,D,F, and S2A). This concurs with the PPARE motifs enriched in our day/night GR cistromes (Figure 1E) and is consistent with PPARα's known role as a direct mediator of circadian lipid metabolism in the liver (Chen and Yang, 2014).

Finally, we detected GR ChIP peaks within the promoter or enhancer regions of all core clock genes (Table S1). We therefore profiled mRNA expression over 24 hours in liver-specific GR knockout mice (Figure S2B&C). Using 'JTK Cycle' to identify mRNAs with robustly oscillating expression profiles, we found that loss of GR caused significant amplitude dampening of rhythmic gene expression across all six time-points (Figure 2G). Specifically, over 1,300 rhythmic mRNAs harboring a nearby GR peak lost oscillation, despite the presence of a functional core clock (Figure 2H). In line with our ChIP-Seq results, the three 'dark' time-points (ZT12, 16, 20) showed more differential gene regulation than the light phase in the GR mutants (Figures 2I, S2B, and S2C). Genes involved in glucose metabolism were downregulated, while lipid, fatty acid and triglyceride metabolism was upregulated at night. Our results suggest that GR interacts with the core clock loop to generate rhythmic output, and that co-regulation of these programs is involved in daily cycles of metabolic adaptation to feeding and fasting (Figure S2D).

High fat diet induces cistromic reprogramming

Prolonged HFD feeding can alter the mammalian circadian clock, for example by disrupting behavioral and molecular rhythms in mice (Kohsaka et al., 2007). We therefore performed analogous GR ChIP-

Seq experiments in mouse livers after 12 weeks of HFD. Importantly, we did not observe significant differences in serum corticosterone concentration in the HFD group, which showed the expected weight gain and insulin resistance (Figures S3A-G).

Interestingly, while the general pattern of circadian GR binding was conserved, we found a significant increase in both the number of peaks and the number of tag counts per site, most prominently at night, upon exposure to HFD (Figures 3A-C). For example, the total number of peaks at ZT12 increased by more than 3,000. This amplified intensity of genomic GC action was mainly detected at ZT12, 16 and 20, and led to a gain of GR binding near promoters, thereby altering the normal proximal-distal distribution during the day-night cycle. Although we did not notice any alteration in signal strength during the day (ZT0, 4, 8), we discovered a pronounced enrichment of target gene sets involved in energy metabolism, in addition to the 'housekeeping' programs identified in the light phase of controls (Figures S3B,C). This additional lipid annotation of the rest/fasting phase in our GR cistromes could be a signature of the disrupted energy partitioning that occurs under HFD (Bass, 2016).

Both 'day' (ZT0, 4, 8) and 'night' (ZT12, 16, 20) GR cistromes were again co-enriched for liver specific motifs such as C/EBP, HNF4α, FoxA, PPAR etc. However, the HFD group now additionally featured a STAT5 motif near GREs (Figure 3D). While around 13,000 sites were collectively bound by GR during the night in controls, HFD tissue displayed additional 9,354 GR peaks (Figure 3E). These night-specific gained GR binding sites were associated with genes involved in both glucose and lipid or fatty acid metabolism as well as insulin signaling (Figure 3F). A motif enrichment analysis to identify specific signatures overrepresented in only these >9,000 night-specific HFD-induced GR binding sites again found a STAT consensus motif (Figure 3G). We would like to stress that the newly gained HFD peak sequences did contain GREs, but only the STAT motif was distinct.

RNA-Seq data from the same livers displayed differential mRNA expression for several hundreds of genes near these gained peaks on HFD. Once more, the expression differences of these putative

HFD-induced GR targets were more prominent during the night and were associated with glucose, amino acid, lipid and fatty acid metabolism (Figures 3H&I, and S3I).

In conclusion, HFD reprogrammed hepatic GR cistromes primarily at night during the feeding phase. Increased DNA binding by GR was associated with STAT5 motifs near genes important for glucose, lipid and fatty acid metabolism. Nightly reprogramming occurred despite similar endogenous ligand levels, similar amounts of nuclear GR, CRY1 and CRY2 proteins (Figures S3H&I), and comparable mRNA profiles of *GR, Stat5* and *11β-hydroxysteroid dehydrogenase*, the gatekeeper enzyme that produces active intracellular GCs (see below).

GR, STAT5 and PPARα signaling pathways intersect

Our motif and pathway enrichment searches predicted the involvement of PPAR and STAT signaling in the modulation of GR activity. PPARα is the most prominent PPAR in the liver, acting as a key sensor for nutritional cues such as fatty acids and lipids, and has an integral role in hepatic energy balance (Kersten et al., 1999; Preidis et al., 2017). This makes it a promising drug target for the treatment of hepatic steatosis and fibrosis (Pawlak et al., 2015). It is conceivable that HFD-fed mice show differences in effective PPAR ligand availability due to changes in diet composition or deregulation of metabolic networks.

Stat5 genetically interact with GR in liver homeostasis, and *GR x Stat5* hepatocyte specific double mutant mice develop hepatic steatosis and hepatocellular carcinoma (Engblom et al., 2007; Mueller et al., 2011; Mueller et al., 2012). *In vivo*, Stat5 activity is regulated by pulsatile growth hormone (GH) or cytokine signaling (Baik et al., 2011).

These observations together with the Stat5 motif being prominently enriched in the differential GR bound sequences, prompted us to perform ChIP-Seq for both PPARα and Stat5 in control and HFD livers at ZT12. As expected, motif analyses showed both STAT and PPAR response elements as the top enriched in the corresponding data sets, together with GREs and the typical liver signatures.

Moreover, pathway annotations of the target genes for both factors were indicative of their roles as key regulators of hepatic metabolism, irrespective of diet (Figures S4A-D).

Interestingly, PPARα occupancy remained largely unchanged between control and HFD livers, while STAT5 showed an increased recruitment and an increased overlap with GR on HFD (Figures 4A-C, and S4E). For example, overlap between GR and STAT5 grew from around 4,000 to almost 8,000 peaks upon exposure to HFD. Co-occupancy between GR and PPARα, on the other hand, remained almost constant between 2,000 – 3,000 peaks. Figure 4D shows two examples of metabolic genes co-bound by GR, PPARα and Stat5, the *Pemt* and *Abat* loci. Of course, this does not mean that PPARα transcriptional activity was not altered, i.e. via changes in ligand availability or co-regulator recruitment.

Importantly, these GR-bound *cis*-regulatory elements almost all (>98%) showed enrichment for the active histone H3K27 acetylation mark, which concomitantly increased at ZT12 (compared to ZT0) and under HFD (at ZT12, compared to control diet) (Figures 4D&E, and S4F&G).

Briefly, we found an expansion of both GR and STAT5 cistromes at ZT12 in HFD livers, accompanied by increased histone H3K27 acetylation. While PPARα occupancy was not affected by the diet, GR and STAT5 co-occupancy increased, near genes important for lipid and fatty acid metabolism.

High fat diet induced reprogramming is driven by STAT5

To identify differential factors regulated by HFD or insulin resistance within the transcriptional complex shared by GR and STAT5, we performed ChIP-MS (GR ChIP coupled to mass spectrometry proteomics). Indeed, both STAT5 and the PPARα heterodimer partner RXR were purified in the GR interactomes (Figures 5A and S5A). However, the proteomics experiments did not reveal other relevant candidates that might explain our observed HFD-induced increase in GR & Stat5 co-occupancy. For instance, chromatin remodelers, histone modifying enzymes, co-regulators and transcription factors (such as SWI/SNF, CBP, HNF4α, C/EBP and NCOA5) were co-purified with GR,

as expected (Fletcher et al., 2002; Oakley and Cidlowski, 2013), but these were similarly enriched under both conditions.

Focusing on GR and STAT5 themselves, hepatocyte-specific *GR* and *Stat5* knockout mice on HFD showed that STAT5 occupancy was not affected by the loss of GR, while GR binding at shared, gained sites was significantly reduced in *Stat5* mutants (Figures 5B&C and S5B&C).

In conclusion, we saw that GR, PPARα and STAT5 co-occupied metabolic enhancers in HFD livers, and that enhanced GR binding depended on the presence of STAT5. This observed increase in STAT5-GR co-occupancy might be due to altered JAK/STAT or GH signaling, in insulin resistant, obese animals.

Cistromic reprogramming affects glucose and triglyceride metabolism

To test whether the HFD-induced binding events were functionally relevant, RNA-Seq was performed for ZT0, 4, 8, 12, 16, 20 in hepatocyte-specific *GR* knockouts. Again, more genes were differentially expressed during the night on HFD, corresponding to pathways including lipid, fatty acid, amino acid and carbohydrate metabolism (Figures 6A and S6A&B). Loss of GR once more caused a transcriptional dampening of circadian amplitude across all time-points, with a large proportion of direct GR targets losing oscillation on HFD (Figures 6B and S6C&D).

Moreover, to directly test whether the HFD-induced binding events were functionally relevant, we determined the differential expression of those genes harboring a gained GR peak nearby, specifically during the feeding phase (Figure 6C). Indeed, more than 400 gained targets were de-regulated in the absence of GR, with the upregulation of lipid and fatty acid metabolism being the most prominent. These GR-dependent changes occurred despite similar mRNA expression of the core clock machinery itself (except for *Per1*) (Figure S6D).

In accordance with our NGS profiles, GR mutants were prone to develop hepatic steatosis, which was exacerbated by HFD, and had lower blood glucose levels specifically during the night (Figures 6D&E and S6E&F). Strikingly, circulating triglycerides were lower only during the day, which was more evident on HFD, while liver triglycerides were significantly higher (Figures 6F&G). These physiological changes could be explained by the reduced expression of gluconeogenic genes like *Pck1* or *Pfkfb3*, and by the increased expression of genes involved in lipid and fatty acid utilization and storage, such as *Cd36* and *PPARγ*, in the absence of GR (Figure 6H). *PPARγ* had previously been implicated in circadian remodeling by HFD, in accordance with these observations (Eckel-Mahan et al., 2013).

In sum, we found that GR alters temporal gene expression profiles by sustaining oscillations. We could functionally link these gene expression changes to nearby GR binding events by using hepatocyte-specific *GR* mutants. Several hundreds of genes displayed *de novo* GR binding and GR dependence on HFD. We showed that the pathways targeted by GR are mainly regulating energy homeostasis, and that they control circulating glucose and triglyceride levels distinctly during times of feeding and fasting.

Ligand independent genomic responses on HFD

To further demonstrate that this increase in DNA-bound GR was indeed due to nutritional or pathogenic effects directly on the chromatin level, we treated both HFD and control mice with a single dose of the exogenous GR ligand Dexamethasone (Dex). Animals were injected at ZT0 (lowest endogenous GCs), and livers were processed for GR ChIP-Seq one hour later. As expected, Dex treatment led to a significant increase in GR ChIP signal intensity (compared to untreated mice at ZT0), presumably resulting from increased occupancy in response to ligand. Interestingly, this signal was even higher in HFD livers, as shown in Figure 7A. We found that, compared to controls, there was a gain in both the number of GR ChIP-Seq peaks as well as in the signal strength after HFD feeding

(Figure 7B). Importantly, this confirms that we measured increased GR occupancy in the face of identical ligand levels.

Furthermore, when we harvested livers 4 hours after Dex injection (at ZT4), we detected a diet-specific differential effect on mRNA expression in obese animals (Figure 7C). RNA-Seq revealed several hundreds of deregulated transcripts that responded differently to GR ligand on HFD. These HFD-specific GC responses could be annotated to circadian rhythms, PPARα signaling, lipid and cholesterol metabolism (Figure 7D).

We performed analogous experiments at the peak of GC secretion, injecting mice at ZT12 and harvesting control and HFD livers for ChIP- and RNA-Seq one and four hours later, respectively. Once more, we confirmed the increased GR ChIP-Seq signal in livers from HFD-fed mice, in spite of identical doses of Dex (with two different antibodies, Figure S7A). However, we did not observe major diet-specific mRNA changes in the Dex response at ZT16, conceivably because GR ligand levels are already very high at night (Figure S7B).

Taken together, we observed an augmented response to exogenous GC treatment on HFD, with identical ligand doses resulting in increased chromatin occupancy of GR at both ZT0 and ZT12. Of note, this altered genomic GC action manifested as differential regulation of metabolic and clock-associated gene expression programs during the fasting period.

Discussion

Rhythmic GR binding strengthens transcriptional clock output in mouse livers

We find that GR binding has a distinct daily pattern closely mirroring ligand availability, with low endogenous GC levels leading to promoter proximal binding near ‘housekeeping’ and gluconeogenic genes during the day. In contrast, the nightly GC surge results in GR binding to distant metabolic

enhancers regulating lipid and amino acid metabolism only during the feeding phase. It appears that GR only reaches those distant enhancers at higher hormone concentrations, which in turn allows the control of these metabolic gene networks only when needed. This implies that GCs govern nutrient partitioning and substrate utilization during daily cycles of feeding/fasting.

Our NGS studies show that the majority of diurnally oscillating transcripts are direct GR targets. GR interacts with core clock factors to enlarge and stabilize the amplitude of downstream target genes. Apparently, GR synchronizes 24 hour rhythms by integrating circadian clock loops with hormone release and by coordinating metabolic fuel shifts. GR reinforces the core Bmal1/Clock/Per/Cry and the ancillary Rev-erb/ROR loops and generates rhythmic outputs (Figure S2E). Our observations again emphasize the tight connection between mammalian circadian rhythms and metabolism.

The nutritional state modifies GC action

Surprisingly, we find that high fat diet expands the GR cistrome, mainly during the feeding phase. This gain in GR ChIP signal was observed despite comparable endogenous corticosterone levels. Although there is a discrepancy in the literature with regard to GC levels in HFD-fed mice (Auvinen et al., 2012; Kohsaka et al., 2007) we did not measure any effect of the diet on the amount of circulating hormones in our cohort. That means that nutrition changes hormone responses at the genomic level, and that we have uncovered a novel way of regulating GR activity independent of ligand availability.

Our observations agree with published studies showing that HFD alters the epigenome and consequently enhancer activity, for example by increasing H3K27 acetylation, DNaseI hypersensitivity and eRNA oscillations (Guan et al., 2018; Leung et al., 2016; Siersbaek et al., 2017; Soltis et al., 2017). Therefore, the enhanced GR occupancy might possibly benefit from increased chromatin accessibility.

This conclusion is further corroborated by the fact that we detected increased GR binding and amplified transcriptional responses in Dex treated mice upon exposure to HFD. Our observations may

have wider implications for human patients being treated with GCs, as one could expect obese or insulin resistant individuals to respond differently to the treatment.

GR & STAT5 interact during cistromic reprogramming

Our studies identified PPARα and STAT5 as interacting with GR in the liver, but we cannot exclude the possibility that other nuclear receptors or transcription factors may also be cross-talking with GR. We focused our analysis on PPARα, for it is a well-known master regulator of hepatic lipid metabolism, and like GR, a fasting-induced receptor (Goldstein et al., 2017; Kersten et al., 1999). However, it is possible that the DR1 motif we identified is bound by other RXR-heterodimerizing nuclear receptors such as other PPARs, FXR or LXRs.

The enrichment of both the STAT5 motif in the GR peaks, as well as the protein itself in the GR interactome, correlate well with the dramatic increase of STAT5 occupancy in HFD livers. Using liver specific mutants, we show that the enhanced GR binding is indeed dependent on STAT5. One possible explanation might be differential post-translational modifications on HFD or rather, insulin resistance. We could not detect any difference in STAT5 Y694 phosphorylation status, the site which is essential for DNA binding and transcriptional activation (Gouilleux et al., 1994), in HFD versus control liver extracts (data not shown). Nonetheless, we cannot rule out the presence of other modifications affecting STAT5 activity. At this point, we do not know whether this augmented GC-JAK-STAT response results from altered cytokine or GH/IGF1/insulin signaling in obese mice, or from changes in the chromatin landscape induced by nutritional adaptation.

Hepatic GR controls glucose and triglyceride metabolism

Finally, we found that the gene programs controlled by GR's temporal occupancy are essential for glucose, lipid and fatty acid metabolism during daily alternations between feeding and fasting.

Hepatocyte specific GR knockouts have lower levels of circulating glucose specifically at night, and lower serum triglycerides during the day. Concomitantly, GR mutants are prone to develop hepatic steatosis. *GR* x *Stat5* liver-specific double mutant mice progress to hepatocellular carcinoma, which might link the GR-STAT5 signature to the development of liver cancer and disease pathology (Mueller et al., 2011).

Altogether, our findings emphasize the key role GR plays for the temporal synchronization of metabolic rhythms in the liver, and highlight its importance during the progression of metabolic disease.

Author Contributions

FQ designed and performed experiments, AAM and KB performed bioinformatic data analyses together with FVF, JH, MH; MW carried out proteomic studies, KAD, CJ and KM performed additional experiments, GDB conducted ChIP experiments and provided feedback, and NHU provided expertise, secured funding, supervised the work and wrote the manuscript.

Acknowledgments

We sincerely thank the NGS Core Facility (HMGU), with S. Lösecke, T. Schwarzmayr, T. Strom and E. Graf; and the MDC genomics core with N. Hübner for their contribution. We are grateful to S. Schön, V. Sportelli, K. Beresowksi, T. Horn, B. Haderlein, M. Mattaboni, T. Müller, K. Biniossek, I. Guderian and S. Regn for assistance. We thank the Tuckermann Lab (Ulm) for GR floxed mice and the Moriggl Lab (Vienna) for Stat5 floxed alleles. This work was supported by funding from the DFG (UH 275/1-1) to NHU, P2LAP3_164906 (SNSF) to CJ and R01 DK108987 (NIH) to GDB.

Declaration of Interests

The authors declare no competing interests.

References

Allhoff, M., Sere, K., J, F.P., Zenke, M., and I, G.C. (2016). Differential peak calling of ChIP-seq signals with replicates with THOR. Nucleic Acids Res *44*, e153.

Auvinen, H.E., Romijn, J.A., Biermasz, N.R., Pijl, H., Havekes, L.M., Smit, J.W., Rensen, P.C., and Pereira, A.M. (2012). The effects of high fat diet on the basal activity of the hypothalamus-pituitary-adrenal axis in mice. J Endocrinol *214*, 191-197.

Baik, M., Yu, J.H., and Hennighausen, L. (2011). Growth hormone-STAT5 regulation of growth, hepatocellular carcinoma, and liver metabolism. Ann N Y Acad Sci *1229*, 29-37.

Balsalobre, A., Brown, S.A., Marcacci, L., Tronche, F., Kellendonk, C., Reichardt, H.M., Schutz, G., and Schibler, U. (2000). Resetting of circadian time in peripheral tissues by glucocorticoid signaling. Science *289*, 2344-2347.

Barclay, J.L., Husse, J., Bode, B., Naujokat, N., Meyer-Kovac, J., Schmid, S.M., Lehnert, H., and Oster, H. (2012). Circadian desynchrony promotes metabolic disruption in a mouse model of shiftwork. PloS one *7*, e37150.

Barnett, D.W., Garrison, E.K., Quinlan, A.R., Stromberg, M.P., and Marth, G.T. (2011). BamTools: a C++ API and toolkit for analyzing and managing BAM files. Bioinformatics *27*, 1691-1692.

Bookout, A.L., Jeong, Y., Downes, M., Yu, R.T., Evans, R.M., and Mangelsdorf, D.J. (2006). Anatomical profiling of nuclear receptor expression reveals a hierarchical transcriptional network. Cell *126*, 789-799.

Chen, L., and Yang, G. (2014). PPARs Integrate the Mammalian Clock and Energy Metabolism. PPAR Res *2014*, 653017.

Cho, H., Zhao, X., Hatori, M., Yu, R.T., Barish, G.D., Lam, M.T., Chong, L.W., DiTacchio, L., Atkins, A.R., Glass, C.K.*, et al.* (2012). Regulation of circadian behaviour and metabolism by REV-ERB-alpha and REV-ERB-beta. Nature *485*, 123-127.

Cui, Y., Riedlinger, G., Miyoshi, K., Tang, W., Li, C., Deng, C.X., Robinson, G.W., and Hennighausen, L. (2004). Inactivation of Stat5 in mouse mammary epithelium during pregnancy reveals distinct functions in cell proliferation, survival, and differentiation. Mol Cell Biol *24*, 8037-8047.

Damiola, F., Le Minh, N., Preitner, N., Kornmann, B., Fleury-Olela, F., and Schibler, U. (2000). Restricted feeding uncouples circadian oscillators in peripheral tissues from the central pacemaker in the suprachiasmatic nucleus. Genes Dev *14*, 2950-2961.

Dobin, A., Davis, C.A., Schlesinger, F., Drenkow, J., Zaleski, C., Jha, S., Batut, P., Chaisson, M., and Gingeras, T.R. (2013). STAR: ultrafast universal RNA-seq aligner. Bioinformatics *29*, 15-21.

Eckel-Mahan, K., and Sassone-Corsi, P. (2013). Metabolism and the circadian clock converge. Physiological reviews *93*, 107-135.

Eckel-Mahan, K.L., Patel, V.R., de Mateo, S., Orozco-Solis, R., Ceglia, N.J., Sahar, S., Dilag-Penilla, S.A., Dyar, K.A., Baldi, P., and Sassone-Corsi, P. (2013). Reprogramming of the circadian clock by nutritional challenge. Cell *155*, 1464-1478.

Engblom, D., Kornfeld, J.W., Schwake, L., Tronche, F., Reimann, A., Beug, H., Hennighausen, L., Moriggl, R., and Schutz, G. (2007). Direct glucocorticoid receptor-Stat5 interaction in hepatocytes controls body size and maturation-related gene expression. Genes Dev *21*, 1157-1162.

Fang, B., Everett, L.J., Jager, J., Briggs, E., Armour, S.M., Feng, D., Roy, A., Gerhart-Hines, Z., Sun, Z., and Lazar, M.A. (2014). Circadian enhancers coordinate multiple phases of rhythmic gene transcription in vivo. Cell *159*, 1140-1152.

Feng, J., Liu, T., and Zhang, Y. (2011). Using MACS to identify peaks from ChIP-Seq data. Curr Protoc Bioinformatics *Chapter 2*, Unit 2 14.

Fletcher, T.M., Xiao, N., Mautino, G., Baumann, C.T., Wolford, R., Warren, B.S., and Hager, G.L. (2002). ATP-dependent mobilization of the glucocorticoid receptor during chromatin remodeling. Mol Cell Biol *22*, 3255-3263.

Goldstein, I., Baek, S., Presman, D.M., Paakinaho, V., Swinstead, E.E., and Hager, G.L. (2017). Transcription factor assisted loading and enhancer dynamics dictate the hepatic fasting response. Genome research *27*, 427-439.

Gouilleux, F., Wakao, H., Mundt, M., and Groner, B. (1994). Prolactin induces phosphorylation of Tyr694 of Stat5 (MGF), a prerequisite for DNA binding and induction of transcription. EMBO J *13*, 4361-4369.

Greulich, F., Hemmer, M.C., Rollins, D.A., Rogatsky, I., and Uhlenhaut, N.H. (2016). There goes the neighborhood: Assembly of transcriptional complexes during the regulation of metabolism and inflammation by the glucocorticoid receptor. Steroids *114*, 7-15.

Guan, D., Xiong, Y., Borck, P.C., Jang, C., Doulias, P.T., Papazyan, R., Fang, B., Jiang, C., Zhang, Y., Briggs, E.R.*, et al.* (2018). Diet-Induced Circadian Enhancer Remodeling Synchronizes Opposing Hepatic Lipid Metabolic Processes. Cell *174*, 831-842 e812.

Heinz, S., Benner, C., Spann, N., Bertolino, E., Lin, Y.C., Laslo, P., Cheng, J.X., Murre, C., Singh, H., and Glass, C.K. (2010). Simple combinations of lineage-determining transcription factors prime cis-regulatory elements required for macrophage and B cell identities. Mol Cell *38*, 576-589.

Hughes, M.E., Hogenesch, J.B., and Kornacker, K. (2010). JTK_CYCLE: an efficient nonparametric algorithm for detecting rhythmic components in genome-scale data sets. J Biol Rhythms *25*, 372-380.

Kersten, S., Seydoux, J., Peters, J.M., Gonzalez, F.J., Desvergne, B., and Wahli, W. (1999). Peroxisome proliferator-activated receptor alpha mediates the adaptive response to fasting. The Journal of clinical investigation *103*, 1489-1498.

Kohsaka, A., Laposky, A.D., Ramsey, K.M., Estrada, C., Joshu, C., Kobayashi, Y., Turek, F.W., and Bass, J. (2007). High-fat diet disrupts behavioral and molecular circadian rhythms in mice. Cell metabolism *6*, 414-421.

Koike, N., Yoo, S.H., Huang, H.C., Kumar, V., Lee, C., Kim, T.K., and Takahashi, J.S. (2012). Transcriptional architecture and chromatin landscape of the core circadian clock in mammals. Science *338*, 349-354.

Kuleshov, M.V., Jones, M.R., Rouillard, A.D., Fernandez, N.F., Duan, Q., Wang, Z., Koplev, S., Jenkins, S.L., Jagodnik, K.M., Lachmann, A.*, et al.* (2016). Enrichr: a comprehensive gene set enrichment analysis web server 2016 update. Nucleic Acids Res *44*, W90-97.

Lamia, K.A., Papp, S.J., Yu, R.T., Barish, G.D., Uhlenhaut, N.H., Jonker, J.W., Downes, M., and Evans, R.M. (2011). Cryptochromes mediate rhythmic repression of the glucocorticoid receptor. Nature *480*, 552-556.

Leung, A., Trac, C., Du, J., Natarajan, R., and Schones, D.E. (2016). Persistent Chromatin Modifications Induced by High Fat Diet. J Biol Chem *291*, 10446-10455.

Li, H., and Durbin, R. (2010). Fast and accurate long-read alignment with Burrows-Wheeler transform. Bioinformatics *26*, 589-595.

Li, H., Handsaker, B., Wysoker, A., Fennell, T., Ruan, J., Homer, N., Marth, G., Abecasis, G., Durbin, R., and Genome Project Data Processing, S. (2009). The Sequence Alignment/Map format and SAMtools. Bioinformatics *25*, 2078-2079.

Liao, Y., Smyth, G.K., and Shi, W. (2014). featureCounts: an efficient general purpose program for assigning sequence reads to genomic features. Bioinformatics *30*, 923-930.

Lim, H.W., Uhlenhaut, N.H., Rauch, A., Weiner, J., Hubner, S., Hubner, N., Won, K.J., Lazar, M.A., Tuckermann, J., and Steger, D.J. (2015). Genomic redistribution of GR monomers and dimers mediates transcriptional response to exogenous glucocorticoid in vivo. Genome research *25*, 836-844.

Love, M.I., Huber, W., and Anders, S. (2014). Moderated estimation of fold change and dispersion for RNA-seq data with DESeq2. Genome Biol *15*, 550.

Marcheva, B., Ramsey, K.M., Peek, C.B., Affinati, A., Maury, E., and Bass, J. (2013). Circadian clocks and metabolism. Handb Exp Pharmacol, 127-155.

Mir, A.A., Dyar, K.A., Greulich, F., Quagliarini, F., Jouffe, C., Hubert, M.J., Hemmer, M.C., and Uhlenhaut, N.H. (2019). In Vivo ChIP-Seq of Nuclear Receptors: A Rough Guide to Transform Frozen Tissues into High-Confidence Genome-Wide Binding Profiles. Methods Mol Biol *1966*, 39-70.

Mueller, K.M., Kornfeld, J.W., Friedbichler, K., Blaas, L., Egger, G., Esterbauer, H., Hasselblatt, P., Schlederer, M., Haindl, S., Wagner, K.U.*, et al.* (2011). Impairment of hepatic growth hormone and glucocorticoid receptor signaling causes steatosis and hepatocellular carcinoma in mice. Hepatology *54*, 1398-1409.

Mueller, K.M., Themanns, M., Friedbichler, K., Kornfeld, J.W., Esterbauer, H., Tuckermann, J.P., and Moriggl, R. (2012). Hepatic growth hormone and glucocorticoid receptor signaling in body growth, steatosis and metabolic liver cancer development. Mol Cell Endocrinol *361*, 1-11.

Nader, N., Chrousos, G.P., and Kino, T. (2009). Circadian rhythm transcription factor CLOCK regulates the transcriptional activity of the glucocorticoid receptor by acetylating its hinge region lysine cluster: potential physiological implications. FASEB journal : official publication of the Federation of American Societies for Experimental Biology *23*, 1572-1583.

Oakley, R.H., and Cidlowski, J.A. (2013). The biology of the glucocorticoid receptor: new signaling mechanisms in health and disease. J Allergy Clin Immunol *132*, 1033-1044.

Oishi, K., Amagai, N., Shirai, H., Kadota, K., Ohkura, N., and Ishida, N. (2005). Genome-wide expression analysis reveals 100 adrenal gland-dependent circadian genes in the mouse liver. DNA Res *12*, 191-202.

Panda, S. (2016). Circadian physiology of metabolism. Science *354*, 1008-1015.

Patel, R., Williams-Dautovich, J., and Cummins, C.L. (2014). Minireview: new molecular mediators of glucocorticoid receptor activity in metabolic tissues. Mol Endocrinol *28*, 999-1011.

Pawlak, M., Lefebvre, P., and Staels, B. (2015). Molecular mechanism of PPARalpha action and its impact on lipid metabolism, inflammation and fibrosis in non-alcoholic fatty liver disease. J Hepatol *62*, 720-733.

Preidis, G.A., Kim, K.H., and Moore, D.D. (2017). Nutrient-sensing nuclear receptors PPARalpha and FXR control liver energy balance. The Journal of clinical investigation *127*, 1193-1201.

Quinlan, A.R. (2014). BEDTools: The Swiss-Army Tool for Genome Feature Analysis. Curr Protoc Bioinformatics *47*, 11 12 11-34.

Reddy, A.B., Maywood, E.S., Karp, N.A., King, V.M., Inoue, Y., Gonzalez, F.J., Lilley, K.S., Kyriacou, C.P., and Hastings, M.H. (2007). Glucocorticoid signaling synchronizes the liver circadian transcriptome. Hepatology *45*, 1478-1488.

Siersbaek, M., Varticovski, L., Yang, S., Baek, S., Nielsen, R., Mandrup, S., Hager, G.L., Chung, J.H., and Grontved, L. (2017). High fat diet-induced changes of mouse hepatic transcription and enhancer activity can be reversed by subsequent weight loss. Sci Rep *7*, 40220.

So, A.Y., Bernal, T.U., Pillsbury, M.L., Yamamoto, K.R., and Feldman, B.J. (2009). Glucocorticoid regulation of the circadian clock modulates glucose homeostasis. Proc Natl Acad Sci U S A *106*, 17582-17587.

Soltis, A.R., Motola, S., Vernia, S., Ng, C.W., Kennedy, N.J., Dalin, S., Matthews, B.J., Davis, R.J., and Fraenkel, E. (2017). Hyper- and hypo- nutrition studies of the hepatic transcriptome and epigenome suggest that PPARalpha regulates anaerobic glycolysis. Sci Rep *7*, 174.

Spiegel, K., Tasali, E., Leproult, R., and Van Cauter, E. (2009). Effects of poor and short sleep on glucose metabolism and obesity risk. Nat Rev Endocrinol *5*, 253-261.

Spiga, F., Walker, J.J., Terry, J.R., and Lightman, S.L. (2014). HPA axis-rhythms. Compr Physiol *4*, 1273-1298.

Takahashi, J.S. (2017). Transcriptional architecture of the mammalian circadian clock. Nature reviews. Genetics *18*, 164-179.

Torra, I.P., Tsibulsky, V., Delaunay, F., Saladin, R., Laudet, V., Fruchart, J.C., Kosykh, V., and Staels, B. (2000). Circadian and glucocorticoid regulation of Rev-erbalpha expression in liver. Endocrinology *141*, 3799-3806.

Wilson, S., Fan, L., Sahgal, N., Qi, J., and Filipp, F.V. (2017). The histone demethylase KDM3A regulates the transcriptional program of the androgen receptor in prostate cancer cells. Oncotarget *8*, 30328-30343.

Wilson, S., Qi, J., and Filipp, F.V. (2016). Refinement of the androgen response element based on ChIP-Seq in androgen-insensitive and androgen-responsive prostate cancer cell lines. Sci Rep *6*, 32611.

Yamamoto, T., Nakahata, Y., Tanaka, M., Yoshida, M., Soma, H., Shinohara, K., Yasuda, A., Mamine, T., and Takumi, T. (2005). Acute physical stress elevates mouse period1 mRNA expression in mouse peripheral tissues via a glucocorticoid-responsive element. J Biol Chem *280*, 42036-42043.

Yang, X., Downes, M., Yu, R.T., Bookout, A.L., He, W., Straume, M., Mangelsdorf, D.J., and Evans, R.M. (2006). Nuclear receptor expression links the circadian clock to metabolism. Cell *126*, 801-810.

Zhang, Y., Fang, B., Emmett, M.J., Damle, M., Sun, Z., Feng, D., Armour, S.M., Remsberg, J.R., Jager, J., Soccio, R.E.*, et al.* (2015). GENE REGULATION. Discrete functions of nuclear receptor Rev-erbalpha couple metabolism to the clock. Science *348*, 1488-1492.

Figure 1

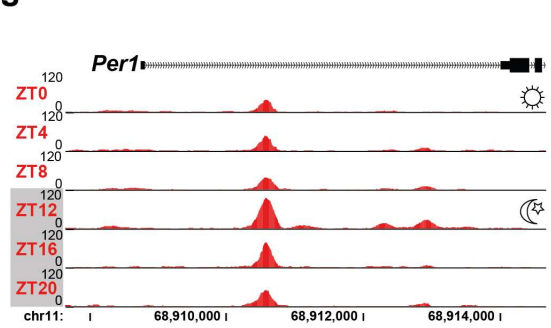

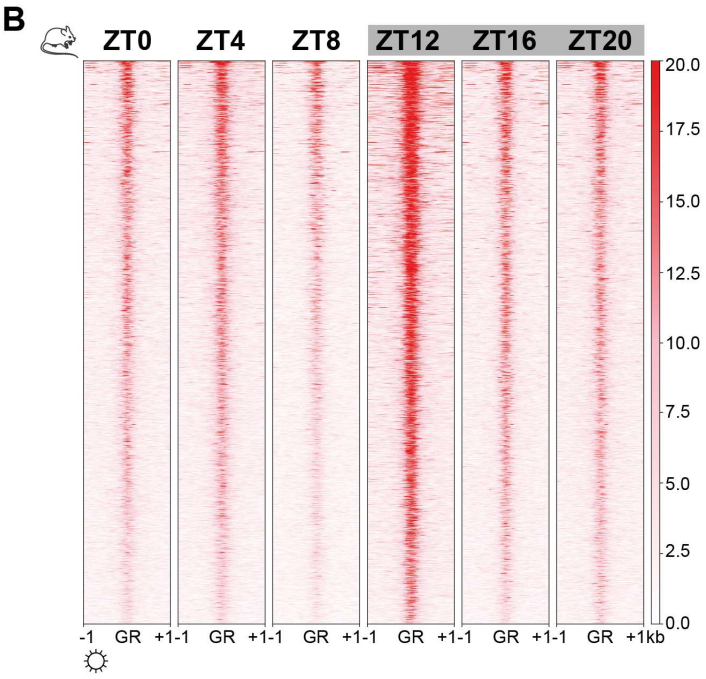

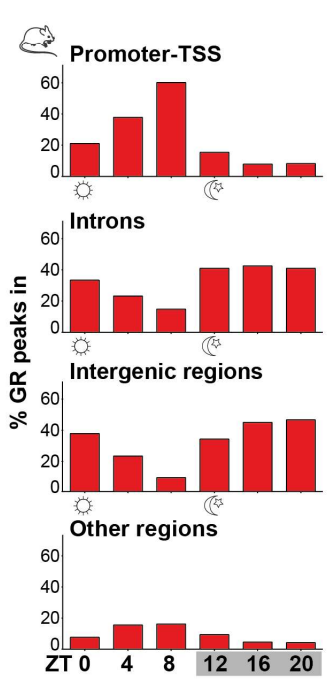

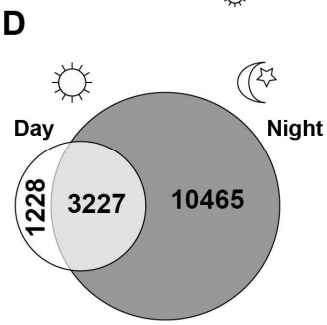

GO (BP): Day	Q-val
protein modification by small protein conjugation	7.9E-26
chromatin modification	5.5E-25
posttranscriptional regulation of gene expression	3.1E-19
cellular response to DNA damage stimulus	4.9E-15
mRNA metabolic process	8.4E-14
protein acetylation	7.3E-12
regulation of glucose metabolic process	1.9E-11

GO (BP): Night	Q-val
lipid metabolic process	6.8E-115
carboxylic acid metabolic process	5.7E-114
oxidation-reduction process	1.1E-79
steroid metabolic process	7.8E-70
fatty acid metabolic process	5.4E-52
cellular amino acid metabolic process	4.0E-38
response to nutrient levels	1.1E-29

E

Day Motif	Factor	p-Value	Night only Motif	Factor	p-Value
	HNF4α	1E-165		HNF4α	1E-568
	C/EBP	1E-125		C/EBP	1E-397
	GR	1E-87		FOX	1E-325
	FOX	1E-81		HNF6	1E-324
	PPAR/RXR	1E-76		PPAR/RXR	1E-281
	HNF6	1E-61		GR	1E-203
	ATF/CREB	1E-40		ATF/CREB	1E-135
	ELK/ETS/ETV	1E-39		HNF1	1E-96

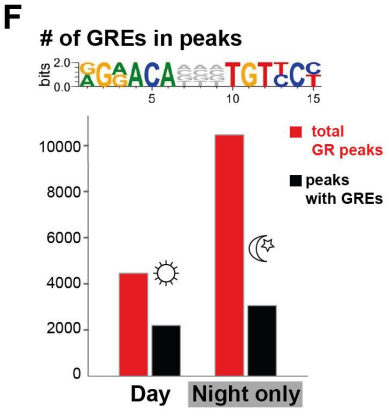

Figure 1. Differences in genomic binding of GR during the day/night cycle in mouse livers

(A) GR occupancy at the *Per1* locus for ZT0, 4, 8, 12, 16 and 20 as determined by ChIP-Seq analysis in mouse livers (normalized tag counts for one representative sample shown). (B) Heatmap of GR genome-wide binding for ZT0-20. Each row shows the normalized unique tag counts for one GR binding event (ChIP peak) of the union (sum of all reproducible peaks from 2 replicates for all 6 time points), ordered by signal strength. (C) GR ChIP peak percent distribution over the indicated genomic regions for the 6 time points. (D): Functional characterization of GR's genomic occupancy during day and night. The 3 time points of the light phase (ZT0, 4, 8 = 'Day') and the dark phase (ZT12, 16, 20 = 'Night') were combined into the Venn diagram. The majority of sites bound during the day (73.1%) were also bound at night. The table displays gene ontology analysis of the genes nearest to the 4,455 'Day' binding sites and the 10,465 'Night only' binding sites. (E) Motif analyses of the 4,455 'Day' and the 10,465 'Night'-specific GR ChIP-sequences for co-occurring hepatic transcription factors. Data presented is from two biological replicates per time point (i.e. a total of 6 samples for each 'Day' and 'Night'). (F): Number of GREs in GR ChIP peaks for 'Day' and 'Night', as defined by the consensus sequence shown.

Figure 2

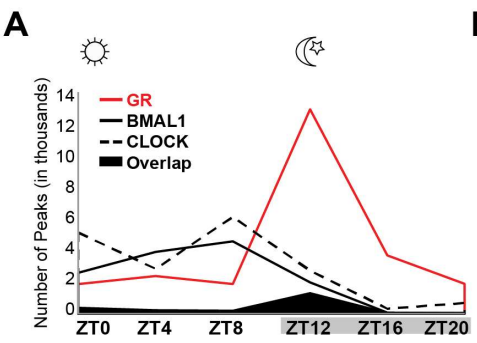

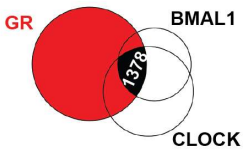

Reactome	Adj P-val
metabolism of lipids and lipoproteins	3.5E-07
metabolism of carbohydrates	9.8E-05
circadian clock	4.2E-04
peroxisomal lipid metabolism	1.7E-03
metabolism of amino acids and derivatives	4.8E-03

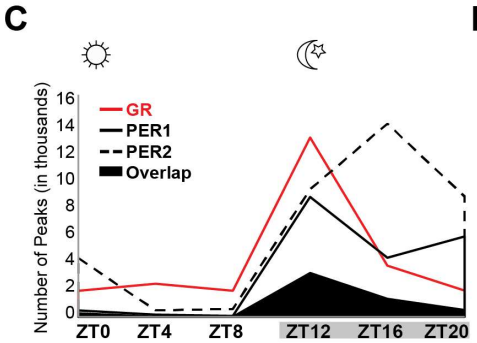

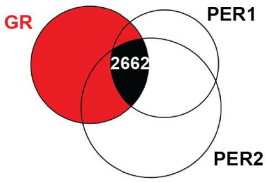

Reactome	Adj P-val
metabolism of lipids and lipoproteins	2.2E-05
circadian clock	4.3E-05
signaling by NOTCH	2.4E-03
nuclear receptor transcription pathway	4.2E-03
metabolism of amino acids and derivatives	1.0E-02

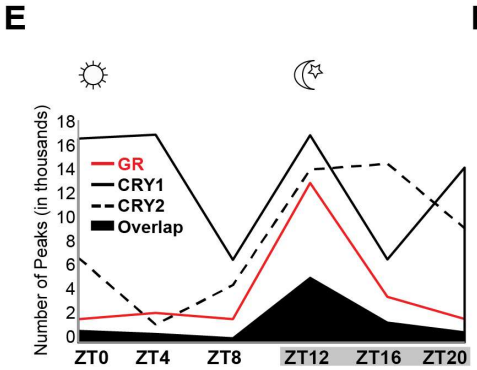

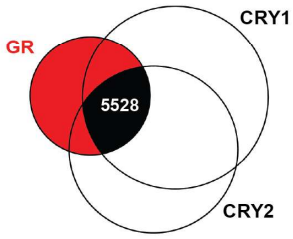

Reactome	Adj P-val
metabolism of lipids and lipoproteins	2.2E-16
regulation of lipid metabolism by PPARα	1.4E-10
circadian clock	3.3E-06
SREBP regulation of cholesterol biosynthesis	2.1E-05
metabolism of amino acids and derivatives	2.2E-05

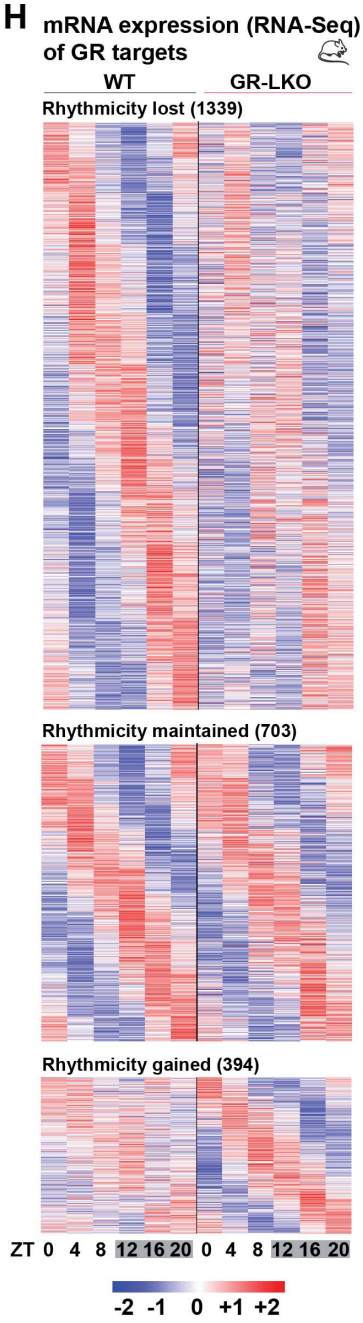

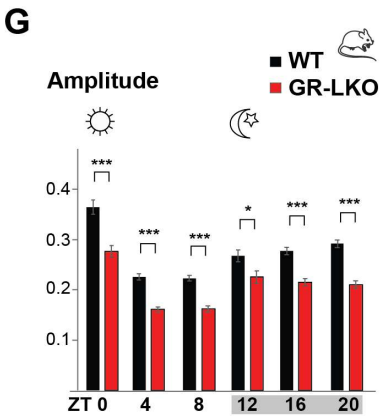

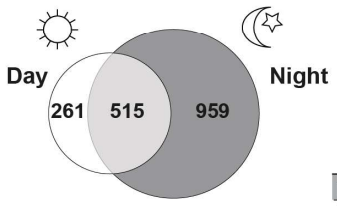

Reactome: down-regulated	Adj P-val
urea cycle	5.6E-03
regulation of complement cascade	1.1E-02
glucocorticoid biosynthesis	3.0E-02
metabolism of amino acids and derivatives	4.3E-02
Reactome: up-regulated	**Adj P-val**
cell cycle	1.7E-06
DNA replication	2.2E-06
nonsense mediated decay	8.8E-06
infectious disease	3.0E-04
translation	4.0E-04
metabolism of proteins	8.1E-03
glutathione conjugation	2.3E-02

Reactome: down-regulated	Adj P-val
glucose metabolism	6.8E-02
retinoid metabolism and transport	6.8E-02
gluconeogenesis	7.5E-02
lipoprotein metabolism	7.5E-02
metabolism of fat soluble vitamins	7.5E-02
synthesis of bile acids and bile salts	1.0E-01
Reactome: up-regulated	**Adj P-val**
triglyceride biosynthesis	5.0E-06
fatty acid, triacylglycerol, and ketone body metabolism	5.1E-05
metabolism of lipids and lipoproteins	1.3E-04
extracellular matrix organization	1.3E-04
cell cycle	1.5E-04
DNA repair	2.1E-03
glycerophospholipid biosynthesis	7.0E-03
collagen formation	7.2E-03

Figure 2. GR binding overlaps with core clock factors to generate transcriptional rhythms

Phase distributions, as number of peaks per time point, for GR with BMAL1/CLOCK (A), PER1/2 (C), and CRY1/2 (E). Co-bound sites are solid black. Venn diagrams depict the GR union from all time points (14,920 sites) intersecting with unions for BMAL1 (6,184) and CLOCK (9,294) (B); PER1 (12,534) and PER2 (20,944) (D); and CRY1 (34,581) and CRY2 (28,658) (F). Functional annotation of *cis*-regulatory sites bound by all three factors (black) is in the tables below (Koike et al., 2012). (G) Amplitude distribution for ZT0-20 in livers from GR-LKO (*Alb-Cre x* $GR^{f/f}$) compared to $GR^{f/f}$ littermates (WT). 3,400 genes cycling in control mice were binned according to peak time point (4hrs). Values are represented as mean ± SEM (n=3 per group). (H) Phase sorted heatmap of oscillating transcripts in WT and GR-LKO livers for ZT0, 4, 8, 12, 16 and 20, n=3. (I) Venn diagram showing number of differentially regulated genes in GR-LKO during the 'Day' (ZT0, 4, 8) and during the 'Night' (ZT12, 16, 20). Pathway annotation was performed for transcripts either up- or down-regulated in GR-LKO. **P*<0.05, ****P*<0.001 (two tailed t test).

Figure 3

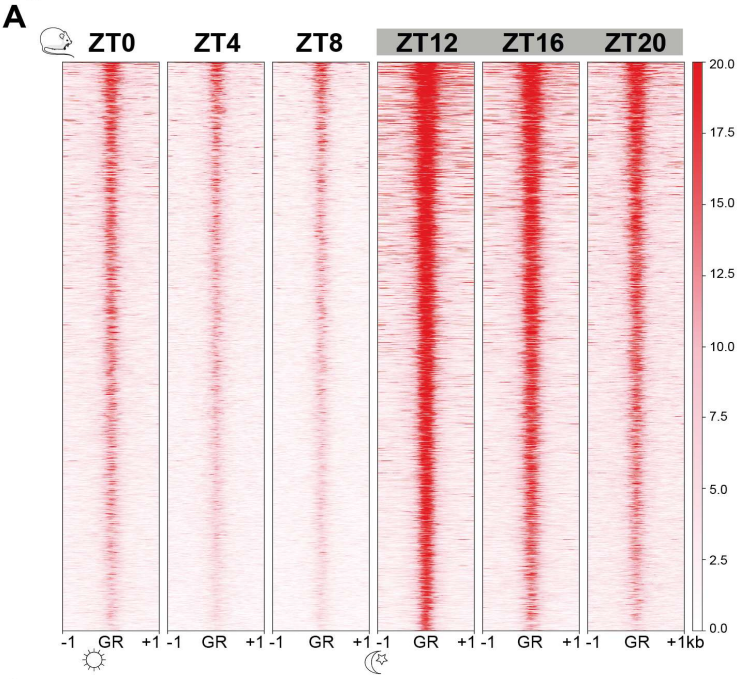

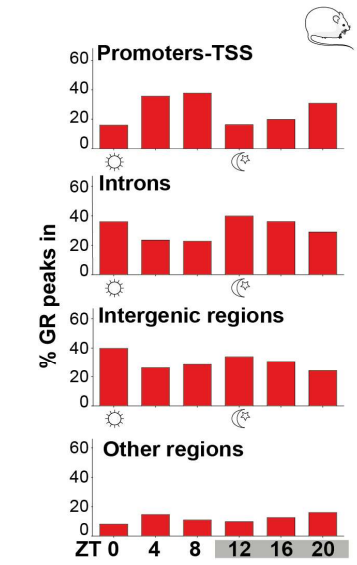

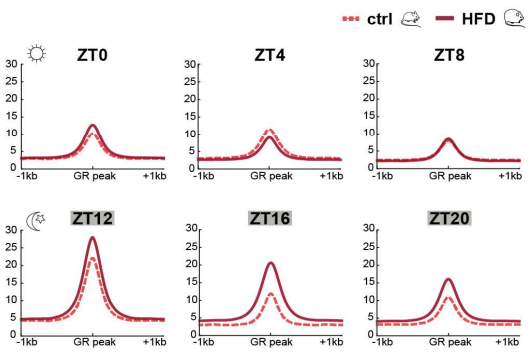

D

Day Motif	Factor	p-Val.	Night only Motif	Factor	p-Val.
	HNF4α	1E-194		HNF4α	1E-694
	C/EBP	1E-129		C/EBP	1E-465
	GR	1E-104		PPAR/RXR	1E-340
	FOX	1E-92		FOX	1E-316
	PPAR/RXR	1E-91		HNF6	1E-284
	HNF6	1E-71		GR	1E-139
	ATF/CREB	1E-51		ATF/CREB	1E-125
	HNF1	1E-32		STAT5	1E-98

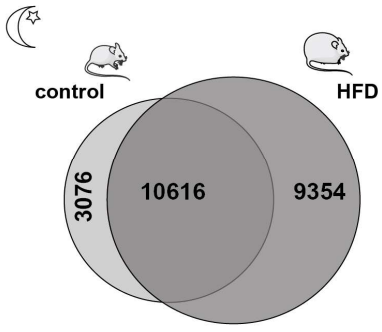

F

GO (BP): Gained peaks	Q-Val
carboxylic acid metabolic process	3.7E-55
fatty acid metabolic process	1.2E-41
lipid biosynthetic process	8.7E-29
response to insulin stimulus	7.6E-24
steroid metabolic process	3.8E-23
regulation of glucose metabolic process	2.8E-22
intrinsic apoptotic signaling pathway	6.9E-12

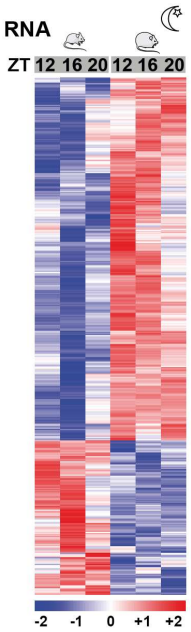

G

Motif	Factor	p-Value
	STAT5	1E-21
	STAT3	1E-9

I

Reactome: down-regulated	Adj P-val
interferon signaling	1.8E-03
peptide chain elongation	2.1E-03
metabolism of carbohydrates	3.8E-03
glucose metabolism	4.9E-03
metabolism of amino acids and derivatives	3.3E-02
Reactome: up-regulated	**Adj P-val**
metabolism of lipids and lipoproteins	1.4E-09
fatty acid, triacylglycerol & ketone body metabolism	1.7E-08
metabolism of amino acids and derivatives	2.8E-07
peroxisomal lipid metabolism	8.6E-07
branched-chain amino acid catabolism	4.6E-06
TCA cycle and respiratory electron transport	1.1E-04
mitochondrial fatty acid beta-oxidation	2.7E-04
fatty acyl-CoA biosynthesis	2.3E-03
pentose phosphate pathway	8.9E-03
pyrimidine metabolism	1.3E-02

Figure 3. GR cistromes are reprogrammed by HFD

(A) Heatmap of GR genome-wide binding for ZT0-20 in livers after 12 weeks HFD. Each row shows the normalized unique tag counts for one GR ChIP peak of the union (sum of all reproducible peaks of the HFD data set), ordered by signal strength. (B) GR ChIP peak percent distribution over the indicated genomic regions for ZT0-20 on HFD. (C) Normalized distribution of GR ChIP-Seq tag density in HFD and control cistromes for the 6 time points. (D) Motif analyses of the 3,258 'Day' and the 16,954 'Night'-specific HFD GR ChIP-sequences show co-occurring hepatic transcription factors. (E) Venn diagram comparing the GR ChIP peak overlap for the sum of all 3 'Night' samples (ZT12, 16, 20) from HFD and control livers. (F) GREAT functional annotation based on the nearest genes of the 9,345 additional HFD GR binding sites. (G) Enriched motifs in the GR ChIP peaks gained on HFD during the dark phase over the GR union used as background. Data presented is from two biological replicates per time point. (H) Heatmap of transcripts associated with gained GR binding from figure 3D (9,354) and deregulated by HFD during the night (ZT12,16,20). (I) Pathway annotation for transcripts either up- or down-regulated in HFD livers.

Figure 4

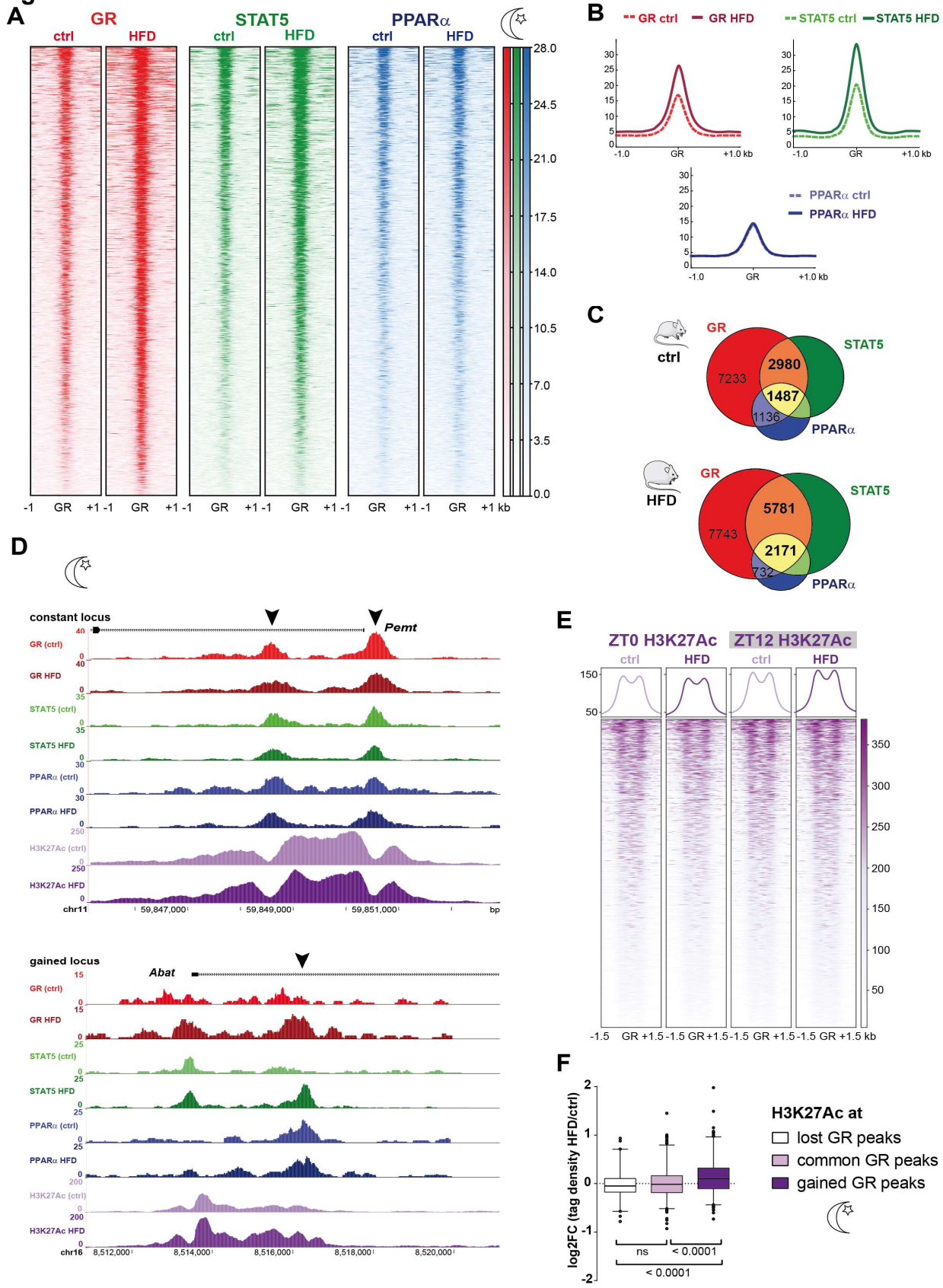
A
GR
STAT5
PPARα
ctrl
HFD
-1 GR +1 kb
B
GR ctrl
GR HFD
STAT5 ctrl
STAT5 HFD
PPARα ctrl
PPARα HFD
C
ctrl
GR
STAT5
PPARα
7233
2980
1487
1136
HFD
7743
5781
2171
732
D
constant locus
Pemt
gained locus
Abat
GR (ctrl)
GR HFD
STAT5 (ctrl)
STAT5 HFD
PPARα (ctrl)
PPARα HFD
H3K27Ac (ctrl)
H3K27Ac HFD
chr11
chr16
bp
E
ZT0 H3K27Ac
ZT12 H3K27Ac
F
log2FC (tag density HFD/ctrl)
ns
< 0.0001
H3K27Ac at
lost GR peaks
common GR peaks
gained GR peaks

Figure 4. GR, PPARα and Stat5 signaling pathways intersect at functional enhancers

(A) Heatmap of GR, Stat5 and PPARα genome-wide binding in control and HFD livers at ZT12. Each row shows the normalized unique ChIP-Seq tag counts for GR, STAT5 and PPARα centered on the GR peak positions and ordered by signal strength. (B) Normalized distribution of GR, STAT5, PPARα ChIP-Seq tag density in control and HFD livers at ZT12, at sites occupied by GR. (C) Venn diagram of GR (12,836 and 16,427 peaks), STAT5 (8,815 and 14,216 peaks) and PPARα (4,317 and 4,438 peaks) cistromes at ZT12 in control and HFD, respectively. (D) Representative examples of normalized GR, STAT5, PPARα and H3K27ac ChIP-Seq tracks in both control and HFD at ZT12. Top: The *Pemt* locus was not affected by diet. Bottom: The *Abat* locus gained GR-STAT5 co-occupancy together with increased H3K27ac on HFD. (E) ChIP-Seq profiles for H3K27ac centered around GR peaks at ZT0 and ZT12 in HFD and control livers. Each row shows the normalized H3K27ac ChIP-Seq tag counts ordered by signal strength. The box plot below is the log2 fold change between HFD and control tag density of H3K27ac ZT12 signal mapped to either the 'lost' (3,076), 'common' (10,616), or 'gained' (9,354) GR sites from Figure 3D. Only peaks near transcripts up-regulated by HFD during the night were used. *P* values according to Mann-Whitney test.

Figure 5

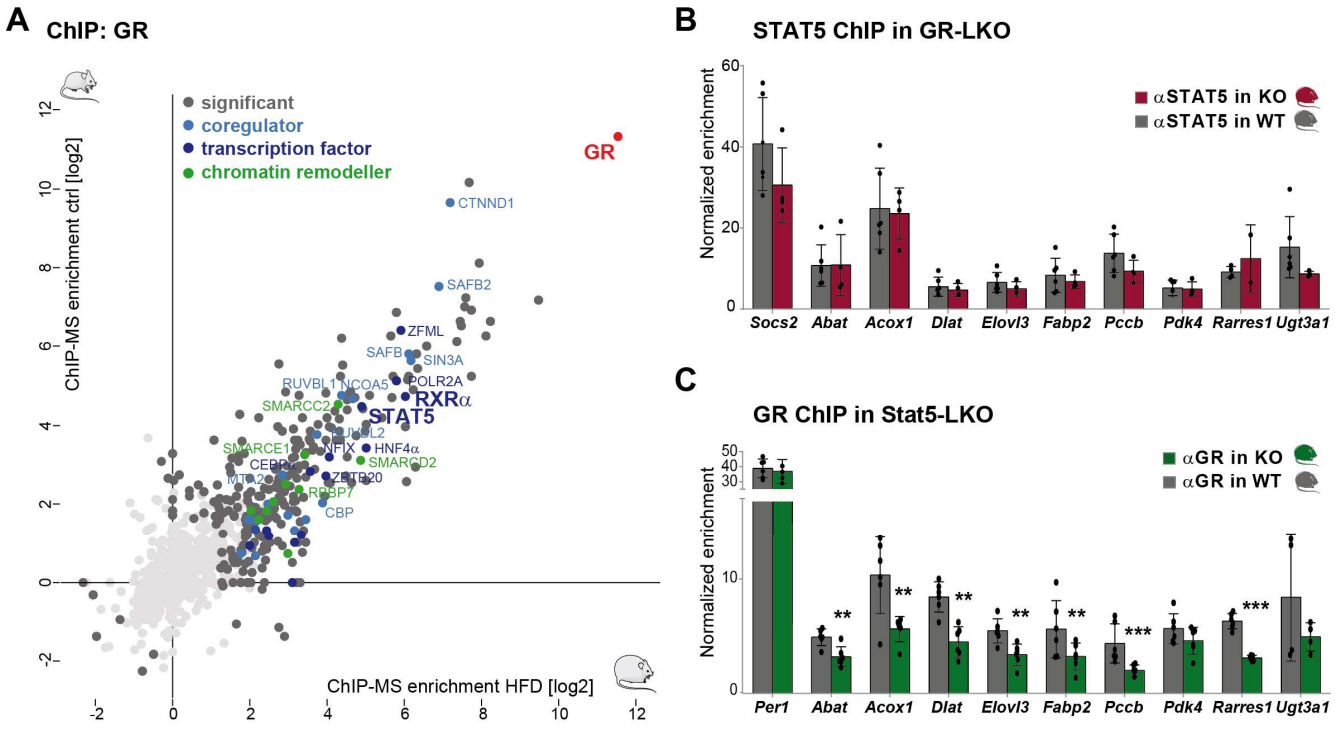
A
ChIP: GR
significant
coregulator
transcription factor
chromatin remodeller
GR
CTNND1
SAFB2
ZFML
SAFB
SIN3A
RUVBL1
NCOA5
POLR2A
SMARCC2
RXRα
STAT5
RUVBL2
XRN2
SMARCE1
XRCC5
HNF4α
CEBPA
SMARCD2
MTA2
ZBTB20
RBBP7
CBP
ChIP-MS enrichment ctrl [log2]
ChIP-MS enrichment HFD [log2]
B
STAT5 ChIP in GR-LKO
αSTAT5 in KO
αSTAT5 in WT
Normalized enrichment
Socs2
Abat
Acox1
Dlat
Elovl3
Fabp2
Pccb
Pdk4
Rarres1
Ugt3a1
C
GR ChIP in Stat5-LKO
αGR in KO
αGR in WT
Normalized enrichment
Per1
Abat
Acox1
Dlat
Elovl3
Fabp2
Pccb
Pdk4
Rarres1
Ugt3a1

Figure 5. Cistromic reprogramming by HFD is driven by STAT5 occupancy

(A) GR interactomes (ChIP-MS) in HFD and control livers at ZT12. Enrichment (Log2 Fold Change) of GR IP samples versus IgG (n=3), was calculated for control and HFD diet samples (Fisher´s exact test, FDR<0.05, s0=1). (B) STAT5 ChIP-qPCR in GR-LKO (*Alb-Cre x* $GR^{f/f}$) and WT ($GR^{f/f}$) livers on HFD. The *Socs2* locus is a positive control for STAT5 binding that was not changed by HFD; the other loci showed HFD-induced gained GR-STAT5 co-occupancy by ChIP-Seq. (C) GR ChIP-qPCR in Stat5a/b-LKO (*Alb-Cre x* $Stat5^{f/f}$) and WT ($Stat5^{f/f}$) livers on HFD. The *Per1* locus is a positive control for GR binding that was not changed by HFD; the other loci are the same as above. Enrichment is calculated over a negative locus. Values are shown as mean ± SEM (n=2-6 per group), $^{**}P<0.01$, $^{***}P<0.001$ (two tailed t test).

Figure 6

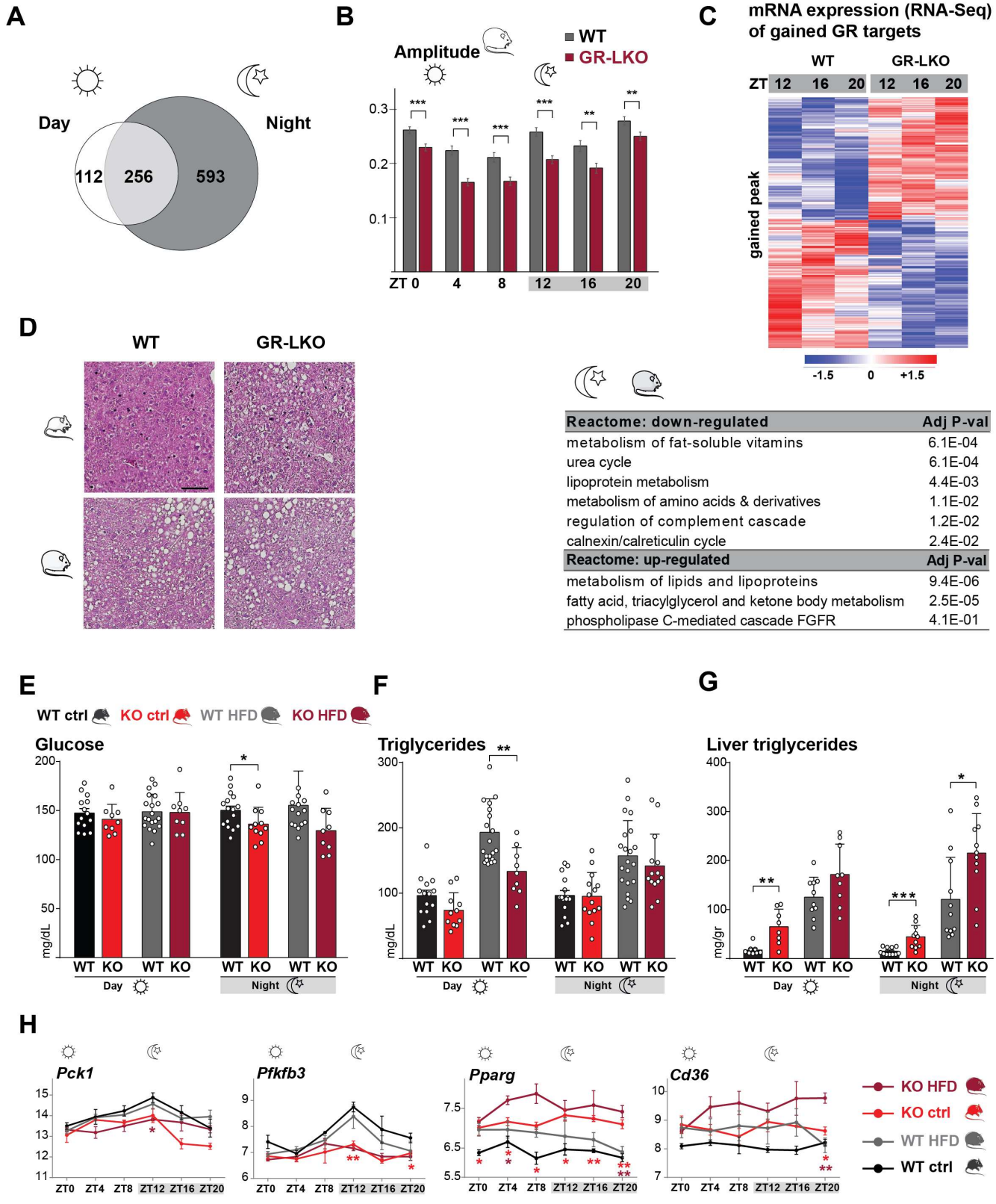
A
Day
Night
112
256
593
B
Amplitude
WT
GR-LKO
0.3
0.2
0.1
ZT 0
4
8
12
16
20
C
mRNA expression (RNA-Seq)
of gained GR targets
WT
GR-LKO
ZT 12 16 20 12 16 20
gained peak
-1.5
0
+1.5
D
WT
GR-LKO
Reactome: down-regulated | Adj P-val
metabolism of fat-soluble vitamins | 6.1E-04
urea cycle | 6.1E-04
lipoprotein metabolism | 4.4E-03
metabolism of amino acids & derivatives | 1.1E-02
regulation of complement cascade | 1.2E-02
calnexin/calreticulin cycle | 2.4E-02
Reactome: up-regulated | Adj P-val
metabolism of lipids and lipoproteins | 9.4E-06
fatty acid, triacylglycerol and ketone body metabolism | 2.5E-05
phospholipase C-mediated cascade FGFR | 4.1E-01
E
WT ctrl
KO ctrl
WT HFD
KO HFD
Glucose
mg/dL
WT KO WT KO WT KO WT KO
Day
Night
F
Triglycerides
mg/dL
G
Liver triglycerides
mg/gr
H
Pck1
Pfkfb3
Pparg
Cd36
ZT0 ZT4 ZT8 ZT12 ZT16 ZT20
KO HFD
KO ctrl
WT HFD
WT ctrl

Figure 6. Liver specific GR mutants show deregulation of glucose and triglyceride metabolism

(A) Venn diagram showing number of differentially regulated genes in GR-LKO (*Alb-Cre x GR$^{f/f}$*) during the 'Day' (ZT0, 4, 8) and during the 'Night' (ZT12, 16, 20) after 12 weeks HFD. (B) Amplitude distribution for ZT0-20 in livers from GR-LKO compared to GR$^{f/f}$ littermates (WT) on HFD. Values are represented as mean ± SEM (n=3 per group). (C) Heatmap of deregulated transcripts in GR-LKO during the night (ZT12,16,20) associated with 'gained' (9,354) GR peaks from figure 3D. Pathway annotation was performed for transcripts either up- or down-regulated in GR-LKO livers. (D) H&E staining of livers from GR-LKO mice and littermate controls after 12 weeks of high fat or control diet. One representative section from n=3 biological replicates is shown (scale bar = 100μM). (E) Blood glucose, (F) serum triglycerides, and (G) liver triglycerides from GR-LKO mice and littermate controls during the day (ZT0, 4, 8) or during the night (ZT12,16, 20), on high fat or control diet. Values are represented as mean ± SD (n=8-20 per group). (H) RNA-Seq data (normalized read counts, Rlog) for deregulated gluconeogenic (*Pck1*, *Pfkfb3*) and lipid metabolism (*Pparγ*, *CD36*) transcripts in GR-LKO mice and controls fed with high fat or control diet. Values are represented as mean ± SEM (n=3 per group), **P*<0.05, ***P*<0.01, ****P*<0.001 (two tailed t test).

Figure 7

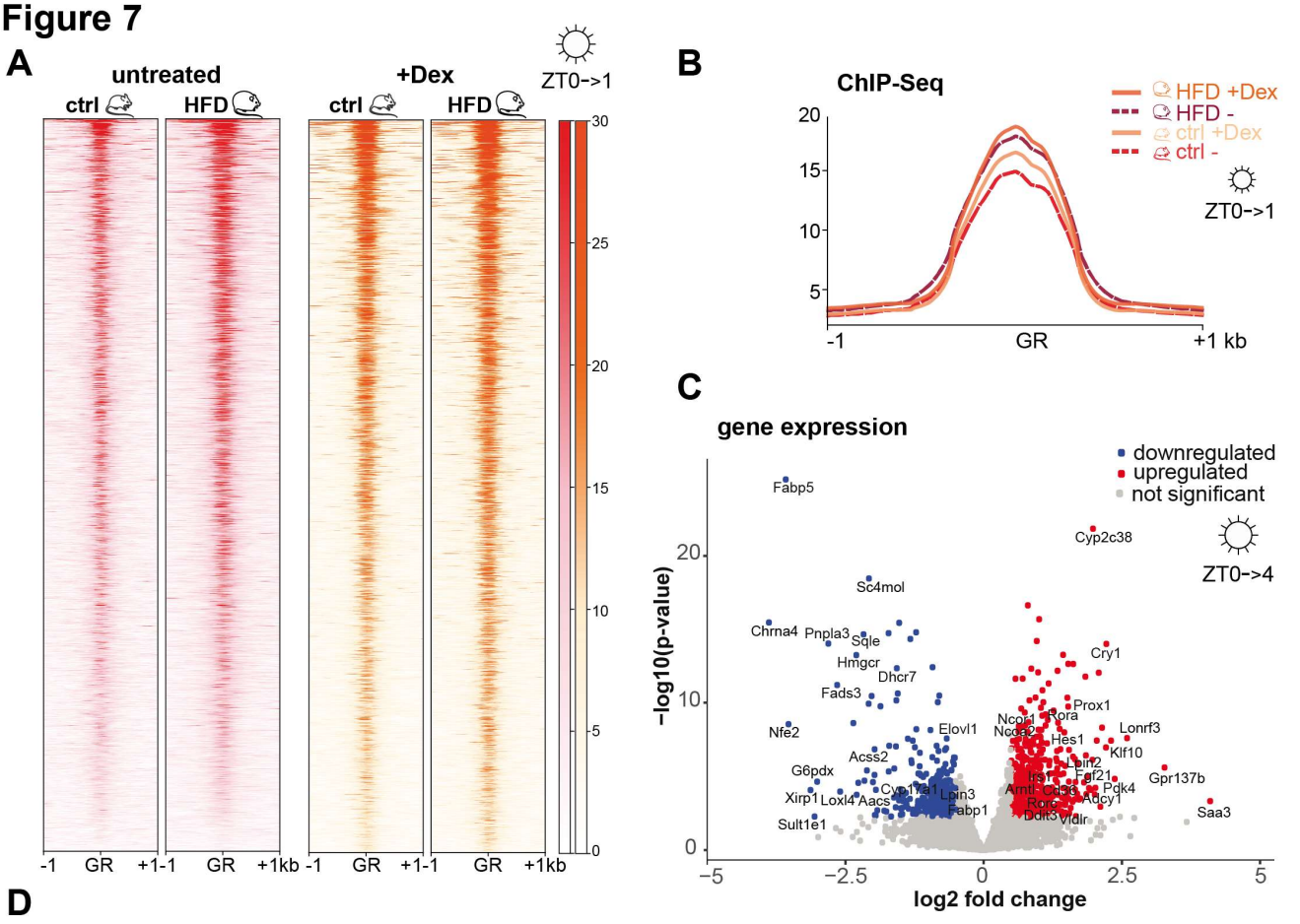

D

Reactome: down-regulated (374)	Adj P-value
cholesterol biosynthesis	1.9E-14
regulation of cholesterol biosynthesis by SREBP	8.4E-07
metabolism of lipids and lipoproteins	1.3E-04
processing of capped intron-containing pre-mRNA	4.3E-04
metabolism of non-coding RNA	2.6E-02
snRNP assembly	2.6E-02
mRNA splicing	2.7E-02

Reactome: up-regulated (608)	Adj P-value
BMAL1:CLOCK,NPAS2 circadian gene expression	4.2E-05
signaling by TGF-beta receptor complex	2.4E-04
ER quality control compartment	2.1E-03
PPARα activated gene expression	2.9E-03
cellular responses to stress	1.3E-02
COPII mediated vesicle transport	1.3E-02
HDMs histone demethylation	1.4E-02

Figure 7. Ligand independent genomic responses on HFD

(A) Heatmap of GR genome-wide binding for Dexamethasone (Dex) treated and control livers, on high fat or control diet. Dex was injected at ZT0 and livers processed at ZT1. Each row shows the normalized ChIP-Seq tag counts ordered by signal strength. (B) Normalized distribution of GR ChIP-Seq tag density, corresponding to A. (C) Volcano plot showing transcripts differentially responding to Dex treatment in HFD versus control (n=2, adj $P<0.05$). Mice were injected with Dex at ZT0 and analyzed at ZT4. (D) Pathway annotation of transcripts down- and up-regulated by Dex treatment in HFD livers compared to controls.

STAR Methods

Further information and requests for resources and reagents should be directed to and will be fulfilled by the Lead Contact, Henriette Uhlenhaut (henriette.uhlenhaut@helmholtz-muenchen.de).

Animal Experiments

Male C57BL/6J mice were housed in a controlled environment (12h light/12h dark daily cycle, ~23°C) and fed either control diet (11 kcal% fat w/sucrose, Research Diets D12329) or High Fat Diet (58 kcal% fat w/sucrose, Research Diets D12331) for 12 weeks. At 18 weeks of age, mice were sacrificed by cervical dislocation, and livers plus blood were collected at the indicated 4 h intervals. Dexamethasone (Sigma, D2915) was administered at ZT0 and at ZT12 as a single i.p. injection of 10 mg/kg after 12 weeks of high fat or control diet. Mice were sacrificed by cervical dislocation 1 h and 4 h later. Hepatocyte-specific *Alb-Cre x GRflox/flox* (Opherk et al. 2004) and *Alb-Cre x Stat5flox/flox* mice (Cui et al., 2004) and controls were placed on High Fat Diet or control diet for 12 weeks. Livers were collected after cervical dislocation. Glucose tolerance tests (GTT) were performed in mice fasted overnight. Glucose (20% D-glucose; Sigma Aldrich) was injected i.p. at 1,5 g/kg and blood glucose levels were determined using a glucometer (AccuCheck Aviva, Roche Diagnostics).

Mouse experiments were performed according to the rules and guidelines established by the Institutional Animal Committee at Helmholtz Center Munich. Ethical approval was received from the local animal welfare authority (District government of upper Bavaria ROB-55.2-2532.Vet_02-14-33)

ELISA

Serum corticosterone was assayed by an enzyme immunoassay kit from Arbor Assays (K014-H1) according to manufacturer's instructions.

Triglyceride assay

For triglyceride measurements, liver tissue was first digested in ethanol / 30% KOH (2:1, v/v) at 60°C. Digested samples were mixed with 1M $MgCl_2$ at a ratio of 1.08:1 (volume) and incubated on ice for 10min followed by centrifugation. Supernatants and serum samples were measured by colorimetric assay (#290-63701, Wako Chemicals) following the company's instructions.

Histology

For H&E staining, 6µm PFA-fixed liver paraffin sections were treated with hematoxylin and eosin Y (#GHS332, Sigma Aldrich) using standard procedures. Brightfield microscopy was performed with a Keyence BZ-9000 microscope at a 10X magnification.

RNA isolation and sequencing

Total RNA was isolated from 50mg of liver using QIAZOL (QIAGEN). Quality of the RNA was assayed using the Agilent RNA 6000 Nano Kit in a 2100 Bioanalyzer (Agilent). Libraries were prepped from 1µg total RNA with the Illumina TruSeq RNA library prep kit v2 chemistry in an automated system (Agilent Bravo liquid handling platform). Libraries were run on a HighSeq4000 sequencer (Illumina).

Chromatin Immunoprecipitation (ChIP)

ChIP was performed as previously described (Uhlenhaut et al. 2013, (Mir et al., 2019)). Briefly, 200mg of frozen liver were minced and Dounce homogenized in 0.7mg/mL DSG crosslinker (Proteochem) and 1% formaldehyde (Thermo Fisher Scientific). Nuclei were isolated and chromatin sonicated to a 0.1-1kb size using a Diagenode Bioruptor. Sheared chromatin was then immunoprecipitated with α-GR antibody (Santa Cruz, sc-1004X; Proteintech, 24050-1-AP), α-PPARα antibody (Santa Cruz, sc-9000), α-Stat5a/b (RD System, AF2168; Cell Signaling, 94205; Abcam, ab194898), α-Stat5a/b (pY694/Y699) (Cell Signaling, 9351) or α-H3K27ac (Abcam, ab4729), and DNA was isolated with MinElute PCR Purification Kits (QIAGEN). DNA concentration was determined by using a QUBIT dsDNA HS kit (Thermo Fisher Scientific).

ChIP-DNA Sequencing

Libraries from ChIP and input DNA were prepared with the KAPA Hyperprep Kit (Kapa Biosystems, KK8504). Illumina compatible adapters were synthesized by IDT (Integrated DNA Technologies) and used at a final concentration of 68nM. Adapter-ligated libraries were size selected (360-610bp) in a Pippin Gel station (Sage Science) using 2% dye free gels (Sage Science, CDF2010). Library concentrations were estimated by RT-PCR with the KAPA Library Quantification Kit (Kapa Biosystems, KK4873). Quality of the libraries was evaluated with the Agilent High Sensitivity DNA Kit in a 2100 Bioanalyzer (Agilent).

ChIP-qPCR

DNA was quantified by use of Power SYBR Green Master Mix (Life Technologies) in a ViiA 7 Real-Time PCR System (Thermo Fischer Scientific). Primers are listed in Table S2.

Total protein extraction

50mg of liver tissue were homogenized in RIPA buffer (150mM NaCl, 1% NP-40, 0.5% sodium deoxycholate, 0.1% SDS, 50mM Tris pH 8.0) supplemented with protease and phosphatase inhibitors.

Nuclear protein extraction

100mg liver tissue were homogenized in buffer containing 10mM Hepes-KOH pH 7.9, 1.5mM MgCl2, 10mM KCl, 0.5mM DTT, 0.15% NP40 with protease and phosphatase inhibitors. After centrifugation, pellets were washed with PBS and nuclei were lysed in 2 vol buffer (10mM Hepes-KOH pH 7.9, 1.5mM MgCl2, 10mM KCl, 0.5mM DTT, 0.1% NP40, 20% glycerol, with protease and phosphatase inhibitors) during 1hr incubation (rotating). After ultracentrifugation, the supernatants constituting the nuclear protein extracts were used for Western blots.

Western blot

10µg (total extracts) and 20µg (nuclear extracts) of lysates were loaded onto a 4-12% Bis-Tris SDS-PAGE gel (Life Technologies) and transferred to a PVDF membrane (Bio-Rad). Western blots were performed according to standard procedure. We used the following antibodies: α-AKT (CST, 4685), α-

AKT (pS473) (Santa Cruz, sc-7985), α-GR (Santa Cruz, sc-393232), α-CRY1 (Abcam, ab104736), and α-CRY2 (kindly supplied by Katja Lamia). Secondary antibodies were: α-rabbit IgG (Santa Cruz, sc-2317), α-mouse IgG (BioRad, 170-6516) and α-guinea pig IgG (Santa Cruz, sc2438).

ChIP-MS

For ChIP experiments followed by mass spectrometry (ChIP-MS), ChIP was performed as described above with minor modifications. For each biological condition, liver samples from 3 mice were pooled. Chromatin was sonicated to an average size of 200bp. Antibody-bait complexes were bound by protein G-coupled Dynabeads (Life Technologies) and washed three times with wash buffer A (50mM HEPES pH 7.5, 140mM NaCl, 1% Triton), once with wash buffer B (50mM HEPES pH 7.5, 500mM NaCl, 1% Triton) and twice with TBS. Precipitated proteins were eluted with an on-bead digest as described before (Hein et al., 2015). Beads were incubated for 30min with elution buffer 1 (2M Urea, 50mM Tris-HCl (pH 7.5), 2mM DTT, 20µg/ml Trypsin) followed by a second elution with elution buffer 2 (2M Urea, 50mM Tris-HCl (pH 7.5), 10mM Chloroacetamide) for 5min. Both eluates were combined and incubated over night at room temperature. Tryptic peptide mixtures were acidified with 1% TFA and desalted with Stage Tips containing 3 layers of C18 reverse phase material and analyzed by mass spectrometry.

Peptides were separated on 50-cm columns packed in-house with ReproSil-Pur C18-AQ 1.9µm resin (Dr. Maisch GmbH). Liquid chromatography was performed on an EASY-nLC 1000 ultra-high-pressure system coupled through a nanoelectrospray source to a Q-Exactive HF mass spectrometer (Thermo Fisher Scientific). Peptides were loaded in buffer A (0.1% formic acid) and separated applying a non-linear gradient of 5–60% buffer B (0.1% formic acid, 80% acetonitrile) at a flow rate of 250nl/min over 105min. Data acquisition switched between a full scan and 15data-dependent MS/MS scans. Multiple sequencing of peptides was minimized by excluding the selected peptide candidates for 25s. All other settings were set as previously described (Scheltema et al., 2014).

Missing values were imputed from a normal distribution applying a width of 0.2 and a downshift of 1.8 standard deviations. Significant outliers were defined by permutation-controlled Student's t-test (FDR < 0.02, s0 =1) comparing triplicate ChIP-MS samples for each antibody and biological condition.

Statistical analysis

Animal experiments were randomized in control and HFD treated groups, individual data point are represented in the plots. In all cases, two tailed tests with P values less than 0.05 were significant. For ChIP-qPCR, multiple t-test was performed with $p<0.05$ (n=2-6 per group). For differences between groups in Rlog counts, multiple t-test was run, with $p<0.05$ (n=3 per group).

Bioinformatics (see Figure S1G)

RNA-Seq:

Pre-processing: RNA-Seq FASTQ files were mapped against the mouse mm9 genome with the STAR v2.4.2a aligner (Dobin et al., 2013). The GENCODE mm9 genome annotation was used. Format conversions were performed using samtools v1.3.1 (Li et al., 2009). The featureCounts program (Liao et al., 2014) was used to count reads located within an exon, do not overlap multiple features, with a threshold of MAPQ >= 4 and are not chimeric.

Normalization and differential expression analysis: The read count matrix was fed into the DESeq2 v1.23.10 program (Love et al., 2014), and variance stabilization was performed to obtain a normalized data matrix. Differential gene expression analysis was performed using a model that quantifies the effect of diet, genotype, time, and their interactions, comparing the different diet-genotype-time groups with each other. The Dex treatment experiment was performed at a single time point. In this case our design formula was: design = ~ diet + treatment + diet:treatment. The number of biological replicates is stated for each comparison.

Oscillating transcript analysis: After normalization, transcript rhythmicity was determined by JTK cycle (Hughes et al., 2010) through the MetaCycle R package (Wu et al. 2016). Circadian cycling was determined over a period of 24h and significant transcripts were selected by using an adjusted p-value <0.05. The groups used for the analysis were hepatocyte-specific *Alb-Cre x* $GR^{fl/fl}$ and littermate $GR^{fl/fl}$ controls, placed on HFD feeding for 12 weeks or control diet.

ChIP-Seq:

Pre-processing: ChIP-Seq FASTQ files were mapped against the mouse mm9 genome with BWA version 7.12 using the MEM algorithm (Li and Durbin, 2010). Duplicate reads were removed using samtools version 0.1.19. Multi mapping reads were removed with bamtools version 2.4.0 using a read threshold of MAPQ >=24 (Barnett et al., 2011).

Adjusting sequencing depth: Sequencing read depth was adjusted by down sampling each replicate BAM file to the replicate with the lowest read count (Table S3).

Peak calling: Macs2 version 2.1.1 was used for peak calling on the replicates using liver genomic DNA as input control (Feng et al., 2011). The peak calling cutoff was set to FDR=0.05. Apart from generating narrow peak files, input normalized read density distributions (Bedgraph) were used for further analysis. Peak boundaries were set by extending the peak summit in either direction by its corresponding library size (calculated from the Bioanalyzer) for each replicate.

Signal artefacts: Peaks falling within pathological repeat elements like satellites, centromeres and telomeric repeats including the ENCODE published black listed regions (https://sites.google.com/site/anshulkundaje/projects/blacklists) were removed from the peak list using Bedtools version v2.25.0 (Quinlan, 2014).

Replicate reproducibility: A customized version of the ENCODE IDR pipeline was used to account for pair-end reads. Pseudo replicates and pairwise correlation analyses were performed among replicate pairs. Peaks within a 200bp summit to summit neighboring distance and ≥50% boundary overlap were merged and marked as confident peaks. Read density plots and Pearson correlation were also

calculated for each replicate to ensure reproducibility. Bedtools version v2.25.0 (Quinlan, 2014) was used to perform the overlap analysis. R version 3.2.3 and Bioconductor were used to create Pearson correlation plots.

Peak Unions: Peak union tables with unique genomic locations from both control and HFD groups were created for GR, STAT5, PPARα, GR-Dex, and H3K27ac data sets. These tables were then combined into a unified peak union with unique ranges across the genome and containing overlapping HFD and control peak information, including the tag count. This table was then used to calculate the peak distribution across the genome and identify peaks of interest, calculating IP efficiency normalization factors.

IP efficiency normalization: ChIP peaks near the promoters of non-changing genes were selected as 'static peaks' (based on RNA-Seq non-differential expression across all HFD and control samples; and based on performance in the different ChIP experiments) (Table S4 and S5). Normalization factors for each replicate were calculated as follows: first, the mean of the non-changing static peaks was calculated for a given region of overlap between peaks (h). Then for a given region (n), the mean of each sample was normalized to a particular signal (hn). Then the normalization factor for each sample would be: Fn = summation of (hn) / total number of control peaks. The count estimate for sample (i) would be: nr = Fn * xi. The normalization factors for each replicate were then used to account for differences in IP efficiency (Table S6). This method is based on the THOR package(Allhoff et al., 2016).

Normalized peak union: Bedgraphs were normalized with the scaling factors obtained from the IP efficiency calculation. Peak calling was then performed on the normalized Bedgraphs with macs2 version 2.1.1 using the bdgpeakcall module with a threshold of p-value 1e-5. To account for false positives, we selected the peaks based on their overlap with the original union. The normalized peak union was then created with normalized tag counts. UCSC tracks were also created using the normalized Bedgraphs.

Normalized read density heatmaps: Normalized bedgraphs were used to plot the read density map near the union peak centers using deepTools version 2.2.4. Replicate groups per time point were first merged using UCSC tools bedGraphToBigWig and bigWigMerge (http://hgdownload.cse.ucsc.edu/admin/exe/macOSX.x86_64/). Then the deepToolscomputeMatrix tool was used, followed by the plotHeatmap tool.

Peak annotation: Peak annotation was performed with HOMER version v4.8 (Heinz et al., 2010). The GENCODE database for mm9 (Release M1) was used as a reference for assigning feature level annotation.

Motif discovery: Two different methods were used for motif discovery: HOMER version v4.8 and a motif analysis based on position site specific matrix models to quantify the utilization of specific hormone response elements (Wilson et al., 2017; Wilson et al., 2016). The ChIP-Seq data was aligned using the ucsc_mm9 reference frame. For individual motif occurrences, a position specific matrix served to compute a log-likelihood ratio score, p values and q values.

Pathway and GO annotation: Pathway enrichment and gene ontology annotation were performed by using the Enrichr and GREAT websites, respectively (Kuleshov et al., 2016McLean, 2010 #323).

ChIP-MS:

Raw mass spectrometry data were analyzed with MaxQuant (version 1.5.3.29) and Perseus (version 1.5.3.0) software packages. Peak lists were searched against the mouse UniprotFASTA database (2015_08 release) combined with 262 common contaminants by the integrated Andromeda search engine. False discovery rate was set to 1% for both peptides (minimum length of 7 amino acids) and proteins. ‘Match between runs’ with a maximum time difference of 0.7min was enabled. Relative proteins amounts were determined by the MaxLFQ algorithm, with a minimum ratio count of two (Cox et al., 2014).

Accession Numbers

The ChIP-Seq and RNA-Seq data sets of this study have been deposited in the GEO (NCBI) database under the SuperSeries accession number GSE108690. Secure token for reviewers: 'kpozmwmoxjedzwx'. Proteomics data have been uploaded to the PRIDE archive (EBI): accession PXD014030.

Excel file 1 GR, H3K27ac, PPARα and Stat5 ChIP-Seq annotated peaks in HFD and control livers.

Excel file 2 Differential gene expression in C57BL/6 livers on control and HFD (DESeq2).

Excel file 3 Rhythmic gene expression in GR-LKO and WT livers, control and HFD (JTKcycle).

Excel file 4 Peptide counts for GR ChIP-MS proteomics in control and HFD livers.

The Supplement contains Figures S1-S7 and Tables S1-S6.